The Radon transform with finitely many angles*

OPEN ACCESS
IOP Publishing
Inverse Problems

Inverse Problems **39** (2023) 105003 (34pp) https://doi.org/10.1088/1361-6420/acef53

The Radon transform with finitely many angles*

Plamen Stefanov

Department of Mathematics, Purdue University, West Lafayette, IN 47907, United States of America

E-mail: Plamen-Stefanov@purdue.edu

Received 16 September 2022; revised 2 August 2023
Accepted for publication 10 August 2023
Published 29 August 2023

Abstract

We study the Radon transform in the plane in parallel geometry possibly undersampled in the angular variable. We study resolution, aliasing artifacts, and edge recovery.

Keywords: Radon transform, sampling, microlocal, edge recovery

(Some figures may appear in colour only in the online journal)

Contents

* P S partially supported by the National Science Foundation under Grants DMS-1900475 and DMS-2154489.

1. Introduction

The purpose of this paper is to study the Radon transform $\mathcal{R}f(\omega,p)$ in 'parallel geometry', see (2.1), in the plane with discrete measurements. We assume that the measurements $\mathcal{R}f(\omega,p)$ are well sampled in the variable p but undersampled in the angular variable ω. This corresponds to practical situations where the measurements are taken at finitely many angles but not as many as needed for good resolution and to avoid aliasing; on the other hand, at each angle, the image is resolved well by a high enough resolution device. We are interested in describing the aliasing artifacts, the resolution limit, and in particular, recovery of edges and jump type singularities.

Sampling $\mathcal{R}f$ pointwise in both variables for $f\in L^\infty_{\text{comp}}$ is not a well posed problem since $\mathcal{R}f$ does not have enough regularity to have well-defined pointwise values, even if f is piecewise smooth. On the other hand, discrete measurements in practice are not done pointwise (even if $\mathcal{R}$ is not a Radon transform) since pointwise, we would measure zero signal with significant noise. Typically, they are locally averaged. In the case of the Radon transform, the x-rays are not ideal rays; they are either collimated and/or issued from a very small source, and additionally blurred by diffraction, see also [3, 35]. When the x-ray projection (as a function of the p variable) is taken at each fixed angle, it is averaged over small detectors (pixels). This is one of the factors limiting the resolution of CT scans used for common medical imaging to the order of 0.5 mm. We refer to [15], for example, for a discussion of the various blur factors affecting the resolution of x-ray based medical imaging. Another reason to assume a slightly regularized $\mathcal{R}f$ is that even with perfect not-yet discretized data, when we want to compute something on a discrete grid, it is beneficial to blur the data a bit before sampling, a common anti-aliasing technique.

The finite number of angles/directions of those projections could be modeled as pointwise measurements of an already locally averaged signal. That averaging can be passed to f by Egorov's theorem, see section 3.2, which allows us to think of pointwise measurements in the

angular variable (not locally averaged) of a slightly blurred copy of f, see [37]. To make things simple, as mentioned above, we assume high enough resolution in the p variable at each fixed angle so that we can assume formally that we have a function known for all p; and this can be justified by the sampling theory [37].

The resulting recovery depends on the way it is done even if we just want to apply the filtered backprojection in a discrete setting. We compare two 'natural' implementations of that formula, and show that they produce different results, in particular each one produces aliasing artifacts, as expected, but they are different. We analyze the method we call 'direct' in more detail since this is the commonly used one. The other one, which we call the 'interpolation' method was already analyzed in [37], and it turns out to produce a reconstruction which is an angularly averaged version of the direct one, see theorem 6.2, making it of lesser interest, probably.

We analyze the problem both with 'classical' and semiclassical (asymptotic) methods. The classical point of view is: how well or not classical singularities are resolved. The most general tool for that would be Fourier integral operators (FIOs) associated with a pair of cleanly intersecting Lagrangians, we refer to remark 4.1(a). More direct methods studying singularities added by a singular cutoff applied to the data, see, e.g. [2, 8, 31] can be used as well, see also theorem 4.1 below. We do not do full analysis—we just study edge recovery, a partial case of recovery of conormal singularities.

The semiclassical (asymptotic) analysis follows in parts the theory developed by the author in [37]: an asymptotic sampling theory as the sampling step tends to zero for FIOs with a canonical relation being locally the graph of a map. The Radon transform is a particular example, and the approach has been applied to Thermoacoustic Tomography as well [26], and to the geodesic x-ray transform [28]. We assume that the sampling step is proportional to a small parameter $h>0$, and use the semiclassical pseudodifferential and FIO calculi. This is one of the technical tools used in this paper. Using it, one can handle undersampling in p as well, as in [37]. Then $\mathcal{R}$ acts on functions depending on h as well, oscillating highly but still smooth. This makes it different than the point of view in [34], for example, where f is fixed but the sampling rate decreases.

We want to emphasize that in sampling theory, the reconstruction from samples depends on the way the interpolation is done, naturally. It could be the Whittaker–Shannon interpolation formula (sinc based) or some version of it if there is oversampling, or even, say linear/bilinear, cubic interpolation, etc. The method we call 'direct' has no interpolation involved, and yet, sampling theory appears naturally through the Poisson summation formula, see section 4. This was unexpected to the author. In particular, the results in [37] do not describe, at least not directly, the reconstruction with or without aliasing.

The semiclassical treatment has the following advantages. Besides modeling dense enough measurements, it is also useful in numerical computations, when the small parameter h is proportional to the step size (when using a mesh). Next, classical microlocal analysis is asymptotic in the sense that it cares about the Taylor-like expansion of the Fourier transform at the infinite sphere $|\xi|=\infty$. Roughly speaking, it misses what happens on the way there. An oscillating function, like $\cos(kx)$ with $k\to\infty$, for example, is smooth, thus negligible in classical microlocal sense. In a semiclassical sense, it has semiclassical singularities, and it is not an approximate classical singularity in any reasonable sense; in fact, its weak limit is zero, as $k\to\infty$.

It is known that $\mathcal{R}$, restricted to finitely many directions, has a non-trivial kernel, see, e.g. [12]. In [22], see also [24], Louis studies the 'ghosts', i.e. the null-space. In [23], he describes the ghosts in all dimensions as a high-frequency phenomenon, generalizing previous works. This is close in spirit to our asymptotic approach but the methods and the conclusions we get are

of a very different nature. Other approaches are based on *a priori* knowledge or assumptions, see, e.g. [11]. Sampling for the Radon transform has been studied in [3, 6, 29, 30, 33], and more recently in [28, 37], and by Katsevich [16–20]. His approach is different from ours, and the conclusions cannot be compared directly. This work was inspired in part by a conversation by the author and him. The author thanks François Monard for the discussions and for the [22, 23]. The anonymous referees helped improve the exposition.

We present a brief outline of the paper. In section 2 we present some basic facts about the Radon transform, the main assumptions and the goal, especially in the asymptotic part. We present some basic facts about the semiclassical analysis in section 3, and about the asymptotic sampling theory developed in [37]. Section 4 describes a commonly used reconstruction method with discrete data that we call 'direct,' and we describe what it recovers. In general, the reconstruction is a distribution, see theorem 4.2 and section 7, even if f is piecewise smooth. The result in theorem 4.2(a) is formally new but easy to obtain, not really the main focus of the paper. Theorem 4.2(b) derives another representation which the author has not seen in the literature and brings us closer to the asymptotic analysis later. The proof is based on the Poisson summation formula. We present this theorem in order to compare them to the asymptotic results, and as a preparation for them. Section 5 is an asymptotic version of the previous one: what happens if the angular step tends to zero, and the sampled functions are allowed to have a finer and finer detail (reflected in the asymptotic nature of $\mathrm{WF}_h(f_h)$). Theorems 5.1 and 5.2 are some of the main results in the paper. Theorem 5.2 in particular, shows that if the Nyquist condition is satisfied, the 'direct' recovery provides a reconstruction up to $O(h^\infty)$ despite the fact that there is no Whittaker–Shannon interpolation, which is required by sampling theory!

2. Preliminaries

2.1. The filtered backprojection

We work in the plane. The Radon transform is defined by

$$\mathcal{R}f(\omega,p)=\int_{x\cdot\omega=p} f(x)\,\mathrm{d}\ell, \tag{2.1}$$

where $\mathrm{d}\ell$ is the Euclidean length measure, and $\omega\in S^1$, say parameterized as

$$\omega(\varphi):=(\cos\varphi,\sin\varphi). \tag{2.2}$$

We denote by $\omega^\perp=(-\omega_2,\omega_1)$ its rotation by $\pi/2$. We always think that $\varphi\in[0,2\pi]$ is as a parameterization of the circle S^1, i.e. identifying 0 and 2π, i.e. $\varphi\in\mathbb{R}/2\pi\mathbb{Z}$. The Radon transform is even: it is invariant under the map $(\omega,p)\mapsto(-\omega,-p)$, i.e. under $(\varphi,p)\mapsto(\varphi+\pi,-p)$. When we study the microlocal properties of $\mathcal{R}f$, we think of it as a function of (φ,p).

A popular inversion formula is the so-called filtered backprojection

$$f=\mathcal{R}'\mathcal{H}g,\quad g=\mathcal{R}f, \tag{2.3}$$

where $\mathcal{R}'g(x)=\int_{S^1} g(x\cdot\omega,\omega)\,\mathrm{d}\omega$ is the adjoint, $\mathcal{H}=\frac{1}{4\pi}Hd_p$, with $d_p=\partial/\partial p$, and H is the Hilbert transform

$$Hg(p)=\frac{1}{\pi}\,\mathrm{pv}\int\frac{g(s)}{p-s}\mathrm{d}s. \tag{2.4}$$

One of the advantages of this formula is that if $g=\mathcal{R}f$ with f compactly supported, then so is g; and to compute the inversion for x in a compact set for x, we need to compute Hd_p with p and s over a bounded interval (for every φ) only. We note that H is the Fourier multiplier by

$-\mathrm{i}\cdot\operatorname{sgn}(\hat{p})$, therefore $Hd_p = |D_p|$, where $D_p = \frac{1}{\mathrm{i}}d_p$. We denote by $\hat{\varphi}$ and $\hat{p}$ the variables dual to φ and p, respectively.

2.2. Discrete data

Assume we are given the Radon transform $\mathcal{R}f(\omega,p)$ sampled on a (finite) discrete set of angles $\{\omega_i\}$. We always assume that $\operatorname{supp} f \subset \mathcal{B}(0,R)$ with $R>0$ fixed, where $\mathcal{B}(0,R)$ is the ball with center 0 and radius R.

We consider the following two methods of applying the filtered backprojection (2.3) given discrete data. The first one that we call the *interpolation method* is to interpolate $\mathcal{R}f(\omega_j,p)$ to get a function for all 'continuous' (ω,p), and then apply (2.3). This can be done approximately on a finer grid. The second one, which we call the *direct method* is to apply $\mathcal{H}$, and then $\mathcal{R}'$ using a discrete approximations of the latter. This is done by performing a numerical integration by summing up $(\mathcal{H}\mathcal{R}f)(\omega_j, x\cdot\omega_j)$ (i.e. replace the actual integral with the Riemann sums (4.2)), while the interpolation method interpolates $(\mathcal{H}\mathcal{R}f)(\omega_j,p)$ first to $(\mathcal{H}\mathcal{R}f)(\omega,p)$, then sets $p = x\cdot\omega$ and integrates.

To have the flexibility to consider the limited angle problem, let $\psi\in C^\infty(S^1)$ be a cut-off function, and assume we are given

$$g_j(p) = \psi(\omega_j)\mathcal{R}f(\omega_j,p) \tag{2.5}$$

for j in some finite index set. For simplicity, we assume that ψ is even. In fact, since $\mathcal{R}$ is even, we can always symmetrize $\psi\mathcal{R}f$, so this assumption is not restrictive. Then we replace $\mathcal{R}f$ above by $\psi\mathcal{R}f$.

2.3. The asymptotic approach

In [37], we proposed an asymptotic point of view following section 3.2. Say that the sampling rates are proportional to a small parameter $h>0$, and we want to understand the asymptotic behavior as $h\to 0$. In other words, the sampling rate w.r.t. φ is hs, and we call s a *relative* sampling rate. Ignoring possible offsets relative to the origin, we can assume

$$\varphi_j = jhs, \quad \text{and denote} \quad \omega_j = \omega(\varphi_j), \tag{2.6}$$

where j runs over a finite set of integer indices. Since φ parameterizes the unit circle, one has to worry about periodicity or not of the sequence φ_j. We assume:

Assumption 1. The number $\pi/hs =: m$ is an integer.

This restricts h to the set $h\in\{\pi/sm;\ m\in\mathbb{N}\}$ for any $s>0$ fixed. Then the number of the distinct ω_j is equal to $2m$, which determines our index set for j: we can take $j=1,\dots,2m$. That set is even, and since ω_j and $-\omega_j$ define the same families of lines parallel to each one of those directions, we actually have m distinct families of parallel lines. Next, $\mathcal{R}f$ is even, and so is ψ, so we can work with the first half of those ω_j's (so that adding the opposite ones completes the whole set), i.e. $j=1,\dots,m$, as it is usually done.

Part of our analysis is not asymptotic, then one can take h fixed, say $h=1$. Then $\pi/s = m$ is an integer. When we do an asymptotic analysis, we take $h\to 0$, which is to say that m is a large parameter.

In the asymptotic part, we work with functions $f(x)$ depending on h as well, semiclassically band limited in the ball $|\xi|\leqslant B$, see section 3.2. To motivate the interest in such functions, fix a function ψ so that $\hat{\psi}\in C_0^\infty(\mathbb{R})$, and set $\psi_h = h^{-1}\psi(\cdot/h)$. In practice, $\hat{\psi}$ may not be of compact support but can decay fast enough to be considered such with a small error. The locally

averaged measurements are then modeled by $\psi_h *_p \mathcal{R}f$, where $*_p$ is the convolution with respect to the p variable. Egorov's theorem [9, section 8.9.3] implies $\psi_h *_p \mathcal{R}f(x) = \mathcal{R}Q_h f + O(h^\infty)$, where Q_h is an h-ΨDO away from $\xi = 0$ with principal symbol $\psi_h(|\xi|)$. This can be made more explicit with the use of the well-known intertwining property of the Radon transform. This observation has two implications: (1) if f is, say, L^∞ only, and independent of h, then $\tilde{f}_h := Q_h f$ is h-dependent and semiclassically band limited; and (2) we can replace averaged measurements near a discrete set of points by pointwise measurements of $\mathcal{R}\tilde{f}$.

3. Semiclassical sampling

We present briefly some fundamentals about the semiclassical analysis, and the results in [37] about asymptotic sampling.

3.1. Elements of semiclassical analysis

Our main reference for semiclassical analysis is [39] but the reader may also consult [4, 25]; and [9] for the theory of the semiclassical FIOs.

We consider functions $f_h(x)$ depending on $x \in \mathbb{R}^n$ and on a small parameter $h > 0$ as well. Often, we suppress the dependence on h and just write $f_h = f$. What matters for the analysis is their asymptotic behavior as $h \to 0$ but in general, they may not have an actual limit; a typical behavior are high oscillations as $h \to 0$. The semiclassical Fourier transform $\mathcal{F}_h f(\xi) = \hat{f}(\xi/h)$ is just a rescaled classical Fourier transform $\mathcal{F}f$. Even though the semiclassical calculus works on (tempered) distributions, we restrict our attention here to functions called *localized in phase space* in [39], and *semiclassically band-limited* in [37]. Those are functions f_h with the following properties: (i) each one is supported in an h-independent compact set, (ii) f_h is tempered (the H^s norm is polynomially bounded in h^{-1} for some s), and (iii) there exists a compact set $\mathbf{B} \subset \mathbb{R}^n$, so that for every open $U \supset \mathbf{B}$, we have $|\mathcal{F}_h f(\xi)| \leqslant C_N h^N \langle \xi \rangle^{-N}$, for $\xi \notin U$, $\forall N$. Here, $\langle \xi \rangle = (1 + |\xi|^2)^{1/2}$.

Then we say that the set $\mathbf{B}$ is a band limit of f. Depending on the application, when the latter is the ball $\mathcal{B}(0, B)$ for some $B > 0$, then B is called a band limit or when it is the square $[-B, B]^n$, then B is the band limit. Note that the notion of band limit depends on the coordinate system but then the sampling geometry does as well.

It is convenient to consider each such f_h as an equivalence class modulo $O(h^\infty)$ errors in the Schwartz class $\mathcal{S}(\mathbb{R}^n)$ (which conforms with the definition in [39]), which in particular allows non-compact supports but there are always representatives of the class with compact supports as stated above.

Such functions belong to $C_0^\infty(\mathbb{R}^n)$ for every h but as mentioned above, they can oscillate highly when $h \to 0$. The semiclassical wave front set $\mathrm{WF}_h(f)$ is defined as follows.

Definition 3.1. For a tempered f_h, $\mathrm{WF}_h(f_h)$ is the set of points x and co-directions ξ defined as the complement of those (x_0, ξ_0) for which there is $\phi \in C_0^\infty(\mathbb{R}^n)$ with $\phi(x_0) \neq 0$ so that $\mathcal{F}_h(\phi f) = O(h^\infty)$ for ξ near ξ_0.

We say that $g_h = O(h^\infty)$, if $|g_h(x)| \leqslant C_N h^N$ for all $N > 0$ and all $x \in \mathbb{R}^n$. Similarly, we say that $g_h = O_{\mathcal{S}}(h^\infty)$, if such an estimate holds for every seminorm of g in the Schwartz class $\mathcal{S}(\mathbb{R}^n)$.

We call the points $(x, \xi) \in \mathrm{WF}_h(f)$ *semiclassical singularities*. They do not necessarily correspond to actual singularities for general tempered f_h, and never for semiclassically band limited ones since those are smooth. We can interpret $(x_0, \xi_0) \in \mathrm{WF}_h(f_h)$ as a statement that $f(x)$ has an oscillating component near x_0 in the direction of ξ_0 (when $\xi_0 \neq 0$) with a frequency

$|\xi_0|/h$. The semiclassical wave front set is not conic in general. The projection of $\mathrm{WF}_h(f)$ onto the dual variable ξ is called the frequency set $\Sigma_h(f)$. It is, in fact, the smallest band limit **B**. Semiclassically band limited functions have compact semiclassical wave front sets, and compact frequency sets.

An example of semiclassically band limited functions is $f := e^{\mathrm{i}x\cdot\xi/h}\chi(x)$ with $\chi \in C_0^\infty$; then the band limit is $\{\xi\}$ as a set, or $B := |\xi|$ as radius of the smallest (closed) ball centered at zero containing ξ. Then $\mathrm{WF}_h(f) = \operatorname{supp}\chi \times \{\xi\}$. Another example is the coherent state (5.11) with $\mathrm{WF}_h(f) = \{(x_0,\xi_0)\}$ and a band limit $\{\xi_0\}$ as a set, or $B := |\xi_0|$ as a number in the sense above.

When f is independent of h, $\mathrm{WF}_h(f)$ captures the classical wave front set in the following sense: $\mathrm{WF}_h(f) = (\operatorname{supp} f \times \{0\}) \cup \mathrm{WF}(f)$, see [39, p 196]. If $\phi \in \mathcal{S}$, and $\phi_h(x) = h^{-n}\phi(x/h)$, then the Friedrichs mollifier $f_h = \phi_h * f$ restricts ξ in $\mathrm{WF}_h(f)$ to $\operatorname{supp}\hat{\phi}$. This is a way to get f_h out of a singular h-independent $f \in \mathcal{E}'(\mathbb{R}^n)$ with a non-conic $\mathrm{WF}_h(f_h)$; with f_h approximating f, as it is well known from the theory of distributions. If $\hat{\phi} \in C_0^\infty$, f_h is semiclassically band limited with band limit (as a set) $\mathbf{B} = \operatorname{supp}\hat{\psi}$. If $\phi \in \mathcal{S}$ only, this is true with a band limit B up to an error $O(B^{-\infty})$ in any Sobolev space. Note that $\psi_h *$ is an h-ΨDO, see below, with symbol $\hat{\psi}(\xi)$.

Semiclassical pseudodifferential operators (ΨDOs) are defined by

$$Pf(x) = (2\pi h)^{-n} \iint e^{\mathrm{i}(x-y)\cdot\xi/h} p(x,\xi) f(y)\,\mathrm{d}y\,\mathrm{d}\xi, \tag{3.1}$$

where, for every compact set K and α, β, the symbol $p(x,\xi)$, possibly depending on h as well, satisfies

$$|\partial_x^\alpha \partial_\xi^\beta p(x,\xi)| \leqslant C_{K,\alpha,\beta} h^k \langle\xi\rangle^{m-|\beta|} \tag{3.2}$$

for some k and m. We also use the notation $P = p(x,hD)$. Acting on semiclassically band limited functions with a fixed band limit, one can just take a compactly supported p, so the decay in ξ above would be automatic. Then such P would be actually bounded from any Sobolev space $H^s{}_1$ to any other one $H^s{}_2$ with a norm $O(h^{-m+s_1-s_2})$. The calculus of h-ΨDOs is similar to that of classical ones, and we refer to the formulas for sums, composition, adjoint, to [39, section 4]. The most commonly used h-ΨDOs are those with symbols having a formal asymptotic expansion $p(x,\xi) = p_0(x,\xi) + hp_1(x,\xi) + \ldots$. Then p_0 is called the principal symbol of p; well defined on $T^*\mathbb{R}^n$. If $p_0 \neq 0$ in some open set $U \subset T^*\mathbb{R}^n$, then we say that p is elliptic there. Semiclassical ΨDOs preserve or shrink the semiclassical wave front sets; and if they are elliptic in U, they actually preserve it there.

(Local) semiclassical FIOs (h-FIOs) are defined similarly but with a phase function $\phi(x,y,\xi)$, $x \in \mathbb{R}^{n_X}$, $y \in n_Y$, $\theta \in \mathbb{R}^N$, satisfying some non-degeneracy conditions, see [9, 25]:

$$Af(x) = (2\pi h)^{-n} \iint e^{\mathrm{i}\phi(x,y,\theta)/h} a(x,y,\theta) f(y)\,\mathrm{d}y\,\mathrm{d}\theta, \tag{3.3}$$

where, for every compact set K and α, β, the amplitude $p(x,\xi)$, possibly depending on h as well, satisfies estimates similar to (3.2). Similarly to the classical FIOs, a fundamental inherent object associated with any such FIO is its *canonical relation* governing the mapping of semiclassical singularities. To define it, we first consider the characteristic variety $\Sigma_\phi := \{\phi_\theta = 0\}$. Then we set the canonical relation to be $C := \{x, \phi_x, y, -\phi_y\} \cap \Sigma_\phi$. We think of C as a relation, mapping (x,ξ) to all (y,η) so that $(x,\xi,y,\eta) \in C$. The latter does not need to be an actual (single-valued) map; it could map a single (x,ξ) to a set of (y,η). The conditions imposed on C however imply that C is a smooth submanifold of $T^*\mathbb{R}^{n_X} \times T^*\mathbb{R}^{n_Y}$. In this paper, we will have $n_X = n_Y = 2$.

3.2. Semiclassical sampling

We summarize some of the results in [37]. The semiclassical sampling theory developed in [37] is an asymptotic version of the classical one.

3.2.1. Sampling a semiclassically band limited function. For a semiclassically limited function with $\Sigma_h(f) \subset [-B_1, B_1] \times \cdots \times [-B_n, B_n]$, it is enough to know its samples (which number is $O(h^{-n})$) on a uniform rectangular grid of side $s_j h_j$ in each direction, with $s_j < \pi/B_j$, in order to recover f up to an $O(h^\infty)$ error. The reconstruction formula is of interpolation type

$$f_h(x) = \sum_{k\in\mathbf{Z}^n} f_h(s_1 hk_1, \dots, s_n hk_n) \prod_j \chi_j\left(\frac{1}{s_j h}(x^j - s_j hk_j)\right) + O_{\mathcal{S}}(h^\infty)\|f\|, \quad (3.4)$$

with $\chi_j \in C_0^\infty$ so that $\operatorname{supp}\hat{\chi}_j \subset (-\pi, \pi)$, and $\hat{\chi}_j(\pi\xi_j/B_j) = 1$ for $\xi \in \Sigma_h(f)$, under the Nyquist condition $0 < s_j < \pi/B_j$; see corollary 3.3 in [37].

The following results are summarized in section 4 of [37], and proved in the rest of the paper.

3.2.2. Sampling classical FIOs. If A is an FIO (classical), and f is as above, one can determine the smallest box where $\mathrm{WF}_h(Af)$ is contained by studying the canonical relation of A. In particular, this applies to $\mathcal{R}$ and to its left inverse $\mathcal{R}^{-1}$. This allows us to compare the sharp sampling requirements for f and Af (and for $A^{-1}f$ if A is elliptic, associated to a local diffeomorphism, like $\mathcal{R}$).

3.2.3. Resolution limit on f posed by the resolution of Af. Loosely speaking, we view resolution as the highest frequency resolvable. On the other hand, we would allow that resolution to depend on the position x and on the (co-)direction ξ, so ultimately, it would be the largest $\mathrm{WF}_h(f)$ we can recover. To motivate this, say that we work with f so that $\mathrm{WF}_h(f) \subset \mathcal{B}(0,R) \times \mathcal{B}(0,B)$ with some $R > 0$, $B > 0$. Then $\overline{\mathcal{B}(0,B)}$ is the smallest set containing all frequencies ξ of *all such* f in our set of functions f. In other words, $|\xi| \leqslant B$, and we can call B the resolution (limit) of such f. We can apply this to the measurements Af as well. If A is an elliptic classical FIO associated to a diffeomorphic canonical relation, then the parametrix A^{-1} exists, and we may ask ourselves what the resolution limit of f is, posed by that of Af. As explained above, $\mathrm{WF}_h(f) \setminus 0 = C^{-1}(\mathrm{WF}_h(Af) \setminus 0)$ which has a sharp upper bound $C^{-1}(\mathcal{B}(0,R) \times \mathcal{B}(0,B)) \setminus 0$ over all measurements Af by assumption. The results is not a product anymore; and in general, the frequency set (the range of ξ) changes with x. For a fixed x, it is not a ball in general. We interpret this set as the resolution (limit) depending on the position and on the direction posed by a resolution limit of Af which may be uniform, say imposed by the sampling rate.

3.2.4. Local averaging. As mentioned in section 2.3, if $g = \mathcal{R}f$, and g is already band limited in a similar way due to its measurements, or just filtered before inversion to avoid aliasing, assuming perfect data of infinite resolution, this is passed to f by Egorov's theorem. Actually, we do not even need Egorov's theorem for $\mathcal{R}$, but the argument applies to more general operators A that are classical FIOs. Assuming that g is replaced by $\phi_h *_p \mathcal{R}f$ with some ϕ with $\hat{\phi} \in C_0^\infty$, it is enough to show that one can replace f by $f_h = \psi_h * f$ as above with *some* ψ with $\hat{\psi} \in C_0^\infty$. The latter follows easily by the previous paragraph and goes back to [37]. Then

$\phi_h * Af = A\psi_h * f + O(h^\infty)$ in $\mathcal{S}(\mathbb{R}^n)$, i.e. the h-independent f can be replaced by the semi-classically band limited f_h with a negligible error just because we filtered the data, which we can always do, and should do to prevent aliasing when discretizing.

3.2.5. Aliasing. If the Nyquist condition $s_j < \pi/B_j$ is not satisfied, aliasing occurs. For simplicity, assume all B_j equal (can be done by a linear transformation). As in the classical case, frequencies 'fold' over the Nyquist box. The interpolation formula approximates not f_h but

$$Gf := \mathcal{F}_h^{-1}\hat{\chi}(s\cdot)\sum_{k\in\mathbb{Z}^n}\mathcal{F}_h f_h(\cdot + 2\pi k/s). \tag{3.5}$$

When there is a non-trivial contribution from $k \neq 0$, we get aliasing artifacts.

Writing $G = \sum_{k\in\mathbb{Z}} G_k$, we get that each G_k is an h-FIO with a canonical relation given by the shifts

$$S_k : (x,\xi) \longmapsto (x, \xi + 2\pi k/s). \tag{3.6}$$

This FIO preserves the space localization but shifts the frequencies, which can be viewed as changing the direction and the magnitudes of the latter. We identify in this paper canonical relations with the maps they induce.

Assume now that A is elliptic, associated to a local diffeomorphism C, like $\mathcal{R}$. Assume that the measurement Af is aliased, and we apply the parametrix A^{-1}. Then the inversion would be $A^{-1}G_kA$; and by the h-FIO calculus, away from zero frequencies, that is an h-FIO with a canonical relation $C^{-1}\circ S_k \circ C$ acting on $(x,\xi) \in \operatorname{supp}\hat{\chi}(s\cdot + 2k\pi)$. The classical aliasing creates artifacts at the same location but with shifted frequencies. The artifacts here however could move to different locations, as it happens for the Radon transform.

3.3. Notation

We summarize here the notations introduced above for the convenience of the reader. The notion of a *semiclassically band limited function* (depending on h) is introduced in section 3.1, where we also introduce the semiclassical Fourier transform $\mathcal{F}_h$, and the notation $\langle\xi\rangle$. We defined there the notion of a *band limit* either as a set, or as a number, depending on the context. The notion $O(h^\infty)$ is defined right after definition 3.1, and simply means decay faster than $C_N h^N$ for every N, as $h \to 0$. We define the *semiclassical wave front set* $\mathrm{WF}_h(f)$, which elements are called *semiclassical singularities*, in definition 3.1. Its projection $\Sigma_h(f)$ onto the ξ variable is called the *frequency set* of f. Semiclassical pseudodifferential operators are defined in (3.1). Local semiclassical FIOs (h-FIOs) are defined in (3.3). We denote the open ball centered at 0 with radius R by $\mathcal{B}(0,R)$.

4. The direct method, classical (non-asymptotic) view

The method we call 'direct' consists of the following. We take $h = 1$ in this section. The asymptotic analysis as $h \to 0$ will be done in the next one. The step size denoted by s, so $\varphi_j = sj = \pi j/m$. Given the discrete data $\mathcal{R}f(\omega_j, p)$, we compute $\mathcal{H}\mathcal{R}f(\omega_j, p)$ as before, which is an operation in the p variable for any ω fixed. If we knew $\mathcal{H}\mathcal{R}f$ for all ω (and p, of course), the inversion would have been

$$f(x) = \int_{S^1} \mathcal{H}\mathcal{R}f(\omega, x\cdot\omega)\,\mathrm{d}\omega, \tag{4.1}$$

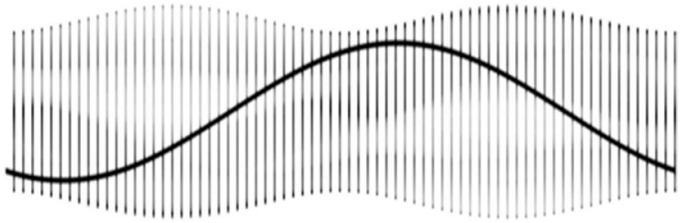

Figure 1. The sinogram of the Shepp–Logan phantom with step size 5°. One first applies $\mathcal{H}$ in the p variable, and then for each x, one computes the integral $\int \mathcal{H}\mathcal{R}f(\varphi, x\cdot\omega(\varphi))\,\mathrm{d}\varphi$ numerically by summing up the values at each angle along the curve representing the lines through x.

which is just (2.3). Instead, we perform numerical integration with the given samples by summing up over ω_j , see figure 1, (and multiplying by the step size $s=\pi/m$) to get

$$f_\delta(x) := \frac{2\pi}{m}\sum_{j=1}^{m}\mathcal{H}\mathcal{R}f(\omega_j, x\cdot\omega_j). \tag{4.2}$$

Note that first, we would get a sum from $j=1$ to $2m$ with the coefficient π/m in front. As noted in the previous section, since $\mathcal{H}\mathcal{R}f$ is even, by assumption 1, we can reduce the summation as indicated and multiply by 2. This is what `iradon` in the current version of MATLAB does, for example. The resulting f_δ would be smooth if f is, which is true for all semiclassically band limited functions.

Consider limited angle data $g=\psi\mathcal{R}f$ now. If we had the non-discretized data, the natural inversion would have been

$$f_\psi(x) := \int_{S^1}\mathcal{H}g(\omega, x\cdot\omega)\,\mathrm{d}\omega = \int_{S^1}\psi(\omega)\mathcal{H}\mathcal{R}f(\omega, x\cdot\omega)\,\mathrm{d}\omega, \tag{4.3}$$

(note that $\mathcal{H}$ commutes with ψ), and with discrete data, we do numerical integration

$$f_{\psi,\delta}(x) := s\sum_j(\mathcal{H}g_j)(\omega_j, x\cdot\omega_j) = \frac{2\pi}{m}\sum_{j=1}^{m}\psi(\omega_j)(\mathcal{H}\mathcal{R}f)(\omega_j, x\cdot\omega_j) \tag{4.4}$$

as in (4.2) instead. The subscript δ can be explained by formula (4.6) below. We are not claiming that (4.3) is the 'best' inversion with limited angle data; in fact this is a problem with a lot of proposed 'solutions' (and without a unique solution [12]). It recovers the singularities stably recoverable from the data however. It follows from [36], for example, that

$$f_\psi = \psi(D/|D|)f. \tag{4.5}$$

The following theorem follows easily from the calculus of wave front sets and the explicit form of the canonical relation of $\mathcal{R}$.

Theorem 4.1. *Let $f\in\mathcal{E}'(\mathbb{R}^2)$. Then $\mathrm{WF}(f_{\psi,\delta})$ is included in the conormals of all lines $\{x;\ (x-x_0)\cdot\omega_j=0\}$ whenever $(x_0,\omega_j)\in\mathrm{WF}(f)$ for some j.*

In other words, all singularities of $f_{\psi,\delta}$ are included in the following set: for every $(x_0,\omega_j)\in\mathrm{WF}(f)$ we take the conormals to the line through x_0 and conormal to ω_j. The examples we present below show that in some cases, this inclusion is actually an equality.

Proof of theorem 4.1. Set

$$(\psi\mathcal{H}\mathcal{R}f)_{\text{int},\delta}(\omega,p)=\frac{2\pi}{m}\sum_{j=1}^{m}\psi(\omega_j)\mathcal{H}\mathcal{R}f(\omega_j,p)\delta(\omega-\omega_j), \tag{4.6}$$

which is as (6.1) below but with $\chi=\delta$, the Dirac delta, there. The Riemann sum (4.4) is the actual integral of the distribution $(\psi\mathcal{H}\mathcal{R}f)_{\text{int},\delta}(\omega,x\cdot\omega)$ in the ω variable, i.e. $f_{\psi,\delta}=R'(\mathcal{H}\psi\mathcal{R}f)_{\text{int},\delta}$. By the calculus of the wave front sets, see, e.g. [13, theorem 8.2.10], the wave front of the product $\mathcal{H}\mathcal{R}f(\omega,p)\delta(\omega-\omega_j)$ is the closure of the vector sum of the wave front set of each factor (the delta considered as a distribution w.r.t. (ω,p)). Note that the product is well-defined since $\text{WF}(\mathcal{R}f)=\text{WF}(\mathcal{H}\mathcal{R}f)$ ($\mathcal{H}$ is elliptic) is separated from the conormals $\lambda\text{d}\varphi$ for f compactly supported, as it follows easily from the expression for the canonical relation of $\mathcal{R}$, see, e.g. [37]. Then the closure of that vector sum is the whole $\mathbb{R}^2\setminus 0$ over every point where $\mathcal{R}f(\omega_j,p)$ is singular. Then all those covectors over any such point would be mapped to singularities conormal to the line $\omega_j\cdot x=p$ by the inverse canonical relation. □

Smooth functions f produce smooth $f_{\psi,\delta}$ by the theorem but even if f is piecewise smooth, $f_{\psi,\delta}$ might be a distribution, not a function, see section 7.

Theorem 4.2. *Assume $f\in\mathcal{S}(\mathbb{R}^2)$, and let $\psi\in C^\infty(S^1)$ be even. Let $f_{\psi,\delta}$, given by (4.4), be the reconstructed f with discrete limited angle data g_j given by (2.5). Then*

(a) $f\mapsto f_{\psi,\delta}$ is the Fourier multiplier (for $\xi\neq 0$)

$$\hat{f}_{\psi,\delta}(\xi)=\frac{\pi}{m}\sum_{j=1}^{m}\psi(\omega_j)\delta\left(\omega_j^{\perp}\cdot\frac{\xi}{|\xi|}\right)\hat{f}(\xi). \tag{4.7}$$

Also,

$$\hat{f}_{\psi,\delta}(\xi)=\frac{\pi}{m}\sum_{j=1}^{m}\delta\left(\omega_j^{\perp}\cdot\frac{\xi}{|\xi|}\right)\left[\psi\left(\frac{\xi}{|\xi|}\right)\hat{f}(\xi)\right], \tag{4.8}$$

thus, $f_{\psi,\delta}$ is a linear operator applied to f_ψ, which is a Fourier multiplier as well.
(b) We also have

$$f_{\psi,\delta}=f_\psi+\sum_{k=1}^{\infty}G_kf_\psi, \tag{4.9}$$

where f_ψ is as in (4.5), G_k are the Fourier multipliers

$$G_k:f\longmapsto\mathcal{F}^{-1}2\cos\left(2mk\arg(\xi)\right)\mathcal{F}f, \tag{4.10}$$

and the series (4.9) converges uniformly and absolutely.

Proof. By the Fourier slice theorem,

$$\mathcal{F}_{p\to\hat{p}}\mathcal{R}f(\omega,p)=\int e^{-\text{i}\hat{p}p}\mathcal{R}f(\omega,p)\,\text{d}p=\int e^{-\text{i}\hat{p}y\cdot\omega}f(y)\,\text{d}y=\hat{f}(\hat{p}\omega).$$

Then

$$\mathcal{F}_{p\to\hat{p}}\psi\,\mathcal{H}\mathcal{R}f(\omega,p)=\frac{1}{4\pi}|\hat{p}|\psi(\omega)\hat{f}(\hat{p}\omega).$$

Therefore,

$$\psi(\omega)\mathcal{H}\mathcal{R}f(\omega,p)=\frac{1}{8\pi^2}\psi(\omega)\int e^{\mathrm{i}\hat{p}p}|\hat{p}|\hat{f}(\hat{p}\omega)\,\mathrm{d}\hat{p}.$$

Hence,

$$(\psi\,\mathcal{H}\mathcal{R}f)(\omega,x\cdot\omega)=\frac{1}{8\pi^2}\psi(\omega)\int e^{\mathrm{i}\hat{p}x\cdot\omega}|\hat{p}|\hat{f}(\hat{p}\omega)\mathrm{d}\hat{p}. \tag{4.11}$$

We apply the definition (4.4) of $f_{\psi,\delta}$ now: we discretize (4.11) to plug it in (4.4), and then take the Fourier transform:

$$\begin{aligned}\hat{f}_{\psi,\delta}(\xi)&=\frac{1}{4\pi m}\sum_{j=1}^{m}\psi(\omega_j)\iint e^{-\mathrm{i}x\cdot\xi+\mathrm{i}\hat{p}x\cdot\omega_j}|\hat{p}|\hat{f}(\hat{p}\omega_j)\,\mathrm{d}\hat{p}\,\mathrm{d}x\\&=\frac{\pi}{m}\sum_{j=1}^{m}\psi(\omega_j)\int\delta(\xi-\hat{p}\omega_j)|\hat{p}|\hat{f}(\hat{p}\omega_j)\,\mathrm{d}\hat{p}.\end{aligned}$$

Split the integral above into one over $[0,\infty)$ and the other one over $[-\infty,0]$, make the change of variables $\hat{p}\mapsto-\hat{p}$, and shift the index j so that $\{\omega_j\}$ gets multiplied by -1 after this. As a result, $\{\omega_j\}_{j=m+1}^{2m}$ are brought up into the sum, and in the second integral, $\hat{p}\in[0,\infty)$. In other words, we can extend the summation to $j=1,\dots,2m$ but restrict the integration to $\hat{p}>0$ only above.

Given a test function ρ, we have

$$\begin{aligned}\langle\hat{f}_{\psi,\delta},\rho\rangle&=\frac{\pi}{m}\sum_{j=1}^{2m}\psi(\omega_j)\int_0^\infty|\hat{p}|\hat{f}(\hat{p}\omega_j)\rho(\hat{p}\omega_j)\,\mathrm{d}\hat{p}\\&=\frac{\pi}{2m}\sum_{j=1}^{2m}\psi(\omega_j)\int_{S^1}\int_0^\infty\hat{f}(\hat{p}\omega)\rho(\hat{p}\omega)\delta\left(\omega_j^\perp\cdot\omega\right)|\hat{p}|\,\mathrm{d}\hat{p}\,\mathrm{d}\omega\\&=\frac{\pi}{2m}\sum_{j=1}^{2m}\psi(\omega_j)\int\hat{f}(\xi)\rho(\xi)\delta\left(\omega_j^\perp\cdot\xi/|\xi|\right)\,\mathrm{d}\xi.\end{aligned}$$

Therefore,

$$\hat{f}_{\psi,\delta}(\xi)=\frac{\pi}{2m}\sum_{j=1}^{2m}\psi(\omega_j)\delta\left(\omega_j^\perp\cdot\xi/|\xi|\right)\hat{f}(\xi),$$

which can be written as (4.7) as well. To gain reader's confidence about this computation, assume $\psi=1$, and note that as $s=\pi/m\to0$, the number of samples $2m$ on the circle is increasing. The formula above converges to $\frac{1}{2}\int\delta(\omega^\perp\cdot\xi/|\xi|)\,\mathrm{d}\omega=1$, multiplied by $\hat{f}(\xi)$, as one would expect. This proves (4.7) in (a). Next, note that on the support of $\delta(\omega^\perp\cdot\xi/|\xi|)$, we have $\omega=\pm\xi/|\xi|$, and the differential of $\omega\mapsto\omega^\perp\cdot\xi/|\xi|$ has norm 1 where that function vanishes. Since ψ is even, this proves (4.8), and completes the proof of (a).

To prove (b), first we want to connect the actual ω integral in (4.3) with its Riemann sum in (4.4) in a Fourier transform kind of way. We consider the one-dimensional version first. The Poisson summation formula implies, say for ρ in the Schwartz class,

$$s\sum_{k\in\mathbb{Z}}\rho(sk)=\sum_{k\in\mathbb{Z}}\hat{\rho}(2\pi k/s), \tag{4.12}$$

where $s>0$ is fixed, and in our case, $s=\pi/m$, as above, see, e.g. [7, section 8.5]. Note that if ρ is a *classically* band-limited function with frequencies in $[-B,B]$, then if $\pi/s>B$ (the Nyquist condition), only the $k=0$ term on the right in (4.12) would be possibly different from zero. Then (4.12) can be interpreted as saying that the Riemann sum on the left, approximating $\int\rho(x)\,\mathrm{d}x=\hat{\rho}(0)$ is exact for such functions. When the Nyquist condition is not satisfied, then (4.12) is exact for the integral of the aliased reconstruction of ρ, and the $k\neq 0$ terms on the right represent corrections coming from the aliased components. Next, notice that the series on the right in (4.12) converges absolutely since $\hat{\rho}$ is in the Schwartz class.

In our case ρ is a 2π periodic function, and we sum over $k\in\mathbb{Z}/2m\mathbb{Z}$ (say, over $k\in\{-m+1,\dots,m\}$). Then in (4.12), $\hat{\rho}$ is evaluated at $2mk$, i.e. those are just Fourier coefficients of ρ; not all of them, just the ones with indices divisible by $2m$. The Poisson summation formula then takes the form

$$\frac{\pi}{m}\sum_{k\in\mathbb{Z}/2m\mathbb{Z}}\rho(\pi k/m)=\sum_{k\in\mathbb{Z}}\hat{\rho}(2mk). \tag{4.13}$$

To get (4.13) from (4.12), we use the partition of unity: there exists $0\leqslant\chi\in C_0^\infty(\mathbb{R})$ so that $\sum_{k\in\mathbb{Z}}\chi(t-2\pi k)=1$ for all s, see, e.g. [7, lemma 8.5.1]. Then we apply (4.12) to $\chi\rho$.

We apply (4.13) to (4.4) with $\rho(\phi):=(\psi\mathcal{H}\mathcal{R}f)(\omega(\varphi),x\cdot\omega(\varphi))$, which is smooth. We get

$$f_{\psi,\delta}=\sum_k f_{\chi,\delta}^{(k)},\quad f_{\chi,\delta}^{(k)}:=\mathcal{F}_{\varphi\to\hat{\varphi}}(\psi\mathcal{H}\mathcal{R}f)(\omega(\varphi),x\cdot\omega(\varphi))\big|_{\hat{\varphi}=2mk}. \tag{4.14}$$

By (4.11), each aliased component in (4.14) is then given by

$$f_{\psi,\delta}^{(k)}(x)=\frac{1}{8\pi^2}\int\int_0^{2\pi}\psi(\omega(\varphi))e^{-\mathrm{i}2mk\varphi}\,e^{\mathrm{i}\hat{p}x\cdot\omega(\varphi)}|\hat{p}|\hat{f}(\hat{p}\omega(\varphi))\,\mathrm{d}\varphi\,\mathrm{d}\hat{p}. \tag{4.15}$$

We split the $\hat{p}$ integration in two parts: over $\hat{p}>0$ and over $\hat{p}<0$. In the second one, we make the change $(\varphi,\hat{p})\mapsto(\varphi+\pi,-\hat{p})$ to get

$$\begin{aligned}f_{\psi,\delta}^{(k)}(x)&=\frac{1}{8\pi^2}\int e^{\mathrm{i}x\cdot\xi}\psi(\xi/|\xi|)e^{-\mathrm{i}2mk\arg(\xi)}\hat{f}(\xi)\,\mathrm{d}\xi\\&\quad+\frac{1}{8\pi^2}\int e^{\mathrm{i}x\cdot\xi}\psi(-\xi/|\xi|)e^{-\mathrm{i}2mk\arg(-\xi)}\hat{f}(\xi)\,\mathrm{d}\xi\\&=\frac{1}{4\pi^2}\int e^{\mathrm{i}x\cdot\xi}\psi(\xi/|\xi|)e^{-\mathrm{i}2mk\arg(\xi)}\hat{f}(\xi)\,\mathrm{d}\xi.\end{aligned} \tag{4.16}$$

Then

$$f_{\psi,\delta}^{(k)}(x)+f_{\psi,\delta}^{(-k)}(x)=\frac{1}{(2\pi)^2}\int e^{\mathrm{i}x\cdot\xi}\psi(\xi/|\xi|)2\cos(2mk\arg(\xi))\hat{f}(\xi)\,\mathrm{d}\xi. \tag{4.17}$$

This completes the proof of (b). □

Remark 4.1.

(a) By (4.7), the map $f_\psi \mapsto f_{\psi,\delta}$ is a formal ΨDO but with a singular symbol. Such operators are studied in [1, 10, 27]. This allows for a point of view more general than that of theorem 4.1. Also, (4.7) can be considered as $\mathcal{R}'\mathcal{R}_b$ with b a singular weight, and the formula is the same when b is smooth, see the appendix in [36].
(b) Each G_k in (4.9) is a ΨDO of order zero, and as such, it does not add additional singularities. The infinite sum however, may, in general, as it is seen from (4.7), see also section 7.
(c) When we view G_k asymptotically, as $m \to \infty$, then G_k are interpreted as semiclassical FIOs for $\xi \neq 0$, when m is considered as a large parameter; which add, and also displace (semiclassical) singularities; see next section.
(d) Formulas (4.7) and (4.9) can be obtained from each other by the Poisson summation formula, as the proof shows.

Remark 4.2. The operator G_k is a convolution with

$$C_{mk}|x|^{-2}\cos(2mk\arg(x)),$$

see [21]. The singularity at $x=0$ is in principal value sense since the cosine function there has a zero mean value over the unit circle.

5. The direct method, an asymptotic view

5.1. The aliasing as a semiclassical FIO

We take the asymptotic view now: the angular step size is sh with $s>0$ fixed and $h \to 0+$. As in theorem 4.2(b) above, according to assumption 1, we assume that $sh = \pi/m$ with $m \in \mathbb{N}$. Then $h \in \{\pi/ms;\ m \in \mathbb{N}\}$ when $s>0$ is fixed, and our analysis is asymptotic, as $m \to \infty$. Formula (4.4) takes the form

$$f_{\psi,\delta}(x) := 2sh\sum_{j=1}^{\pi/hs} \psi(\omega_j)(\mathcal{H}\mathcal{R}f)(\omega_j, x\cdot\omega_j), \quad \omega_j = \omega(shj). \tag{5.1}$$

The function f is assumed to be h-dependent, and semiclassically band limited, see section 3.1, say with $\mathrm{WF}_h(f) \subset \mathcal{B}(0,R)\times\mathcal{B}(0,B)$. Theorem 4.2 still holds but we replace $\hat{f}$ now by its semiclassical version $\mathcal{F}_h f(\xi) = \hat{f}(\xi/h)$. The relevant part is (b) in this case with f_ψ still given by (4.5). It follows from (4.10) that

$$G_k : f \longmapsto \mathcal{F}_h^{-1} 2\cos\frac{2\pi k\arg(\xi)}{sh}\mathcal{F}_h f. \tag{5.2}$$

It is convenient to write the cosine function as a sum of complex exponentials, the way we derived it in the first place:

$$G_k = \mathcal{A}_k + \mathcal{A}_{-k}, \quad \mathcal{A}_k : f \longmapsto \mathcal{F}_h^{-1} e^{2\pi i k\arg(\xi)/sh}\mathcal{F}_h f, \quad k = \pm1, \pm2, \dots. \tag{5.3}$$

We get the sum of two unitary h-FIOs away from the zero section. The phase functions are $\Phi_k(x,y,\xi) = 2\pi k\arg(\xi)/s + (x-y)\cdot\xi$. The characteristic variety $\Sigma_k := \{\partial_\xi \Phi_k = 0\}$ is given by

$$y = x + \frac{2\pi k}{s}\xi^\perp/|\xi|^2.$$

Then $(x,\partial_x\Phi_k)\mapsto(y,-\partial_y\Phi_k)$ on Σ_k is actually a map, so we get that the canonical relation C_k of $\mathcal{A}_k$ are (the graphs of, and we identify them with their canonical transformations)

$$C_k:(x,\xi)\mapsto\Big(x+\frac{2\pi k}{s|\xi|}\frac{\xi^\perp}{|\xi|},\xi\Big). \tag{5.4}$$

This leads to the following theorem; we refer to section 3 for the definition of a semiclassically band limited function.

Theorem 5.1. *Let f_h be semiclassically band limited. Then, given its discretized localized Radon transform $\{g_j\}$ as in (2.5) at $\varphi_j=shj$, $j=1,\dots,2m$, the reconstructed $f_{\psi,\delta}$ by (4.4) has the form*

$$f_{\psi,\delta}=f_\psi+\sum_{k=-\infty,k\neq0}^{\infty}\mathcal{A}_kf_\psi, \tag{5.5}$$

where $\mathcal{A}_k$ are the Fourier multipliers given by (5.3). The operators $\mathcal{A}_k$ are unitary, and away from the zero section, they are elliptic semiclassical FIOs of order zero with canonical relations C_k given by (5.4).

We proved in theorem 4.2 that the series (4.9) converges rapidly, therefore this would be true in the asymptotic case for (5.5) for every fixed $h>0$. In theorem 5.2 below, we estimate how the convergence depends on $h>0$ as well.

Remark 5.1. Theorem 5.1 shows that while artifacts are always created, the original f appears in the expansion as well. *In this sense*, no resolution has been lost! That term f could, in principle overlap or even be canceled by the artifacts of another singularity elsewhere. To avoid aliasing artifacts in a fixed ball $\mathcal{B}(0,R)$, we need $2\pi/(s|\xi|)>2R$, i.e. $s<\pi/BR$. This is the same requirement we got in [37], see also (6.4). This is formulated in theorem 5.2(b) below.

Remark 5.2. If we only look at the canonical relation for $f_{\psi,\delta}$ restricted to $\mathcal{B}(0,R)$, the sum in (5.5) is locally finite. Indeed, since $|\xi|\leqslant B$ by the assumption on f, we have $2\pi/s|\xi|\geqslant 2\pi/sB$, therefore C_k shifts each x at least at distance $2\pi k/sB$, which is a lower bound of the distance of the artifacts to x. Then this would leave any disk $\mathcal{B}(0,R')$ when $2\pi k/sB>R+R'$, i.e. when $k>sB(R+R')/(2\pi)$. We show in the proof of theorem 5.2 below that in fact, only finitely many terms in (5.5) could possibly contribute a non $O(h^\infty)$ addition to $\mathrm{WF}_h(f_{\psi,\delta})\setminus 0$ when $f_{\psi,\delta}$ is restricted to any fixed bounded set. For that, we need an estimate of each term $\mathcal{A}_kf_\psi$ both in k and h.

Theorem 5.2. *Assume that $f=f_h$ is a semiclassically band limited function with $\mathrm{WF}_h(f)\subset\mathcal{B}(0,R)\times\mathcal{B}(0,B)$ for some $R>0$, $B>0$. Then*

(a) Given $R'>0$, restricting k in (5.5) to $|k|\leqslant k_0:=sB(R+R')/(2\pi)$ results in an $O(h^\infty)$ error in $C^m(\overline{\mathcal{B}(0,R')})$ for every m.

(b) As a consequence,

$$\mathrm{WF}_h(f_{\psi,\delta})\setminus 0\subset\bigcup_{k\in\mathbb{Z}}C_k(\mathrm{WF}_h(f_\psi)\setminus 0).$$

(c) If $B>2\pi/(s(R'+R))$, then $f_{\psi,\delta}=f_\psi+O(h^\infty)$ in $C^m(\overline{\mathcal{B}(0,R')})$ for every m. In particular, if $B<\pi/sR$ (the Nyquist condition), then $f_{\psi,\delta}=f_\psi+O(h^\infty)$ in $C^m(\overline{\mathcal{B}(0,R)})$ for every m.

(d) Under the Nyquist condition $B<\pi/sR$ of (c), in the whole $\mathbb{R}^2$,

$$\mathrm{WF}_h(f_{\psi,\delta}-f_\psi)\setminus 0=\bigcup_{k\in\mathbb{Z}\setminus 0} C_k(\mathrm{WF}_h(f_\psi)\setminus 0). \tag{5.6}$$

Proof. Recall that the large parameter m is related to the small one h by $m=\pi/(sh)$. The operator $\mathcal{A}_k$ admits the representation (4.15), excluding ψ there, as shown in (4.16). In other words, rescaling $\hat p$ to $\hat p/h$, we get

$$\mathcal{A}_k f(x)=(8\pi^2h^2)^{-1}\int\int_0^{2\pi}\int e^{\mathrm{i}\Psi_k(x,y,\phi)/h}f(y)\,\mathrm{d}y\,\mathrm{d}\phi\,\mathrm{d}\hat p \tag{5.7}$$

with a phase $\Psi_k:=-2mkh\phi+\hat p(x-y)\cdot\omega(\phi)=-2\pi k\phi/s+\hat p(x-y)\cdot\omega(\phi)$. Since $\Sigma_h(f)\subset\mathcal{B}(0,B)$, and $\Sigma_h(f)$ is compact, then there are $B'<B''<B$ so that $\Sigma_h(f)\subset\mathcal{B}(0,B')$. Let $Q(y,\hat p)$ be a h-ΨDO cutoff with $\operatorname{supp}Q\subset\mathcal{B}(0,R)\times\mathcal{B}(0,B'')$, with $Q=1$ on $\mathcal{B}(0,R)\times\mathcal{B}(0,B')$. Then we can insert the factor $Q(y,\hat p)$ in (5.7) which would result in an $O(h^\infty)$ error. This limits the range of $\hat p$ in (5.7) to $|\hat p|<B''$. Then $\partial_\phi\Psi_k=-2\pi k/s+\hat p(x-y)\cdot\omega^\perp(\phi)$, and for $|k|>k_0$,

$$\begin{aligned}|\partial_\phi\Psi_k|&\geqslant 2\pi|k|/s-B''(R+R')\\&=(B-B'')(R+R')+2\pi(|k|-k_0)/s>C|k|.\end{aligned} \tag{5.8}$$

On the other hand, we have the upper bound

$$|\partial_\phi^m\Psi_k|\leqslant C_m(1+|k|). \tag{5.9}$$

Clearly, $Le^{\mathrm{i}\Psi_k}=e^{\mathrm{i}\Psi_k}$ with $L:=-\mathrm{i}h|\partial_\phi\Psi_k|^{-2}\partial_\phi\Psi_k\cdot\partial_\phi$. Integrating N times in (5.7) w.r.t. ϕ, we derive the estimate

$$\|\mathcal{A}_k f\|_{L^2(\mathcal{B}(0,R'))}\leqslant C_N(h/|k|)^N,\quad k\geqslant k_0,\ \forall N=1,2,\dots. \tag{5.10}$$

Estimate (5.10) implies (a) immediately.

Part (b) now follows directly from (a), theorem 5.1, and from the properties of semiclassical FIOs, see [9, 25].

For statement (c), note that when $2\pi/sB>R'+R$, C_k sends (x,ξ) with $|x|<R$, $|\xi|<B$ outside $\mathcal{B}(0,R')$ (cross $\mathcal{B}(0,B)$) when $k\neq 0$. This also follows directly from (a). Then only the $k=0$ term in (5.5) provides a non-trivial contribution to the sum.

For part (d), note first that the inclusion $\subset$ follows as in (a). To prove the equality, choose $(x^\sharp,\xi^\sharp)$ in the union on the right, say corresponding to $k=k_0$, i.e. $(x^\sharp,\xi^\sharp)=C_{k_0}(x_0,\xi_0)$ for some $(x_0,\xi_0)\in\mathrm{WF}_h(f_\psi)$. Then k_0 and (x_0,ξ_0) with that property are uniquely determined. Indeed, we must have $\xi_0=\xi^\sharp$ (we work in a fixed coordinate system, and comparing covectors at different points makes sense); and there is unique k so that $C_k^{-1}(x^\sharp,\xi_0)=C_{-k}(x^\sharp,\xi_0)$, see (5.4), would land in $\mathcal{B}(0,R)$ since $B<\pi/sR$. This is also true under a small perturbation of $(x^\sharp,\xi^\sharp)$. Next, each $\mathcal{A}_k$ is elliptic, which proves the claim. □

Remark 5.3. We want to emphasize that the equivalent to (c) above in [37] was derived about the interpolation method we discuss in next section, i.e. we have the same about $f_{\psi,\chi}$ we study there. Then the two methods are equivalent when the Nyquist condition holds.

Remark 5.4. The proof of theorem 5.2 (d) reveals something more. The function $f_{\psi,\delta}-f_\psi$ can be regarded as the artifacts under the inversion of $\mathcal{R}$. They lie outside $\mathcal{B}(0,R)$ by part (c). Moreover, they consist of the union of unitary images under $\mathcal{A}_k$ *which do not intersect each*

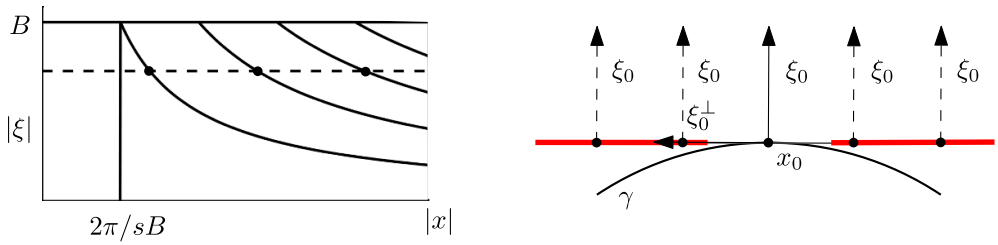

Figure 2. Illustration to the canonical maps C_k of $\mathcal{A}_k$. Left: fixing $|\xi_0|$ (the dashed line), produces a finite number of points along the line through x_0 normal to ξ_0 where x_0 is mapped (with the same ξ). The horizontal axis is the shift relative to x_0 along that line. Right: the image of $(x_0,\xi_0)\in N^*\gamma$.

other in the following sense. Each singularity in the artifact comes from a unique one from $\mathrm{WF}_h(f)$, and micro-localizing near $(x^\sharp,\xi^\sharp)$ allows us to recover f microlocally at the unique pre-image just by applying $\sum\mathcal{A}_k$, which is non-trivial for one k only. In particular, we can recover f up to $O(h^\infty)$ from its artifacts outside $\mathcal{B}(0,R)$.

Remark 5.5. As a corollary, if the singularities are conormal to an edge as in section 8, their artifacts appear conormal to lines tangent to that edge, as in the classical case; and along each such tangent line, they stay at distance at least $2\pi/sB$ from the point of tangency. This is illustrated in figure 2, right. In other words, f_δ is separated from the artifacts, assuming $\mathrm{WF}_h(f)$ small enough. In a typical application of theorem 5.2(d), $\mathcal{B}(0,R)$ is not going to be the computational window, it would be a much smaller neighborhood of a point x_0. Then the theorem applies to f (micro)-localized there. On the other hand, without the localization, the reconstructed f near x_0 could be affected by artifacts caused by singularities farther away.

5.2. Numerical examples

Our first example demonstrates the theorems, with $\psi=1$, and in particular, the role of the magnitude $|\xi|$ of the frequency ξ. We take the 'coherent state'

$$f_h(x;x_0,\xi_0)=e^{\mathrm{i}x\cdot\xi_0/h-|x-x_0|^2/2h} \tag{5.11}$$

with some x_0, $\xi_0\neq 0$ as a test function; more precisely its real part $\Re f_h$. It is well known [39] that $\mathrm{WF}_h(f_h)=\{(x_0,\xi_0)\}$; then $\mathrm{WF}_h(\Re f_h)$ also adds the point $(x_0,-\xi_0)$. In figure 3, row one, we plot a coherent state on the square $[-1,1]^2$ discretized to a 800×800 grid with $|\xi^0|=0.8$, $h=\pi/360\approx 0.0087$, $s=10$, so that $sh=\pi/36$, i.e. the angular step is 5°, corresponding to $m=\pi/hs=36$. The amplitude range in each case is $[-1,1]$, corresponding to the minimum and the maximum of $\Re f_h$; in particular the gray background corresponds to $f=0$. Then (5.4) predicts a shift of the phantom in the direction $\xi^\perp$ at distance $\pi/4\approx 0.7854$ for $k=\pm 1$, which is shown in sub-figure (b) with direct inversion, and in (c) by computing G_kf as the Fourier multiplier (5.2). On the second row, we multiply ξ by 1.7, which decreases the size of the shits by the same factor by (5.4). Finally, on row three, we decrease h by 2. This shrinks the visible size of the phantom by $\sqrt{2}$, compared to the first row, and increases the absolute frequency ξ/h by the same factor because the semiclassical one ξ remains the same.

(a) The original f

(b) Direct inversion with a step $sh = 5^\circ$.

(c) Fourier multiplier inversion, $k = 0, \pm 1$.

(d) The original f; ξ is 1.7 higher

(e) Direct inversion with a step $sh = 5^\circ$.

(f) Fourier multiplier inversion, $-2 \le k \le 2$.

(g) The original f; ξ as in (a) but h halved

(h) Direct inversion with a step $sh = 2.5^\circ/$

(i) Fourier multiplier inversion, $-1 \le k \le 1$.

Figure 3. The direct method. A coherent state, (row one); then the state with ξ multiplied by 1.7 (row two); then as in row one but h is halved. The shifted artifacts stay at distances inversely proportional to $|\xi|$. In row one, $sh = 2\pi/72$ (i.e. 5°).

6. The interpolation method, an asymptotic view

6.1. Asymptotic analysis of the interpolation method

We interpolate the data to a function of the 'continuous' $(\varphi, p) \in [0, 2\pi] \times [-R, R]$ (as usual thinking about $[0, 2\pi]$ as a parameterization of the circle S^1, i.e. identifying 0 and 2π). There are many ways to interpolate discrete data, of course, and our choices are dictated by sampling theory requirements. Once we do that, we invert the data even though the interpolated $\mathcal{R}f$ almost certainly does not belong to the range of $\mathcal{R}$ by applying either the filtered backprojection (2.3) to it or some other operator which is a parametrix of $\mathcal{R}$. Numerically, we can just pass to a finer grid, upsample the data there, and do the inversion. We want to understand the resulting inversion.

Figure 4. The sinogram of a very small Gaussian, sampled at 5° in φ, then interpolated. In the steep parts of the curve, the interpolation is not optimal but it is good along the horizontal ones.

The interpolated data (2.5) then would looks like this:

$$g_{\rm int} = \sum_{j=1}^{\pi/sh} \psi(\omega(jhs))\mathcal{R}f(\omega(jhs),p)\chi\Big(\frac{\varphi - jhs}{hs}\Big), \tag{6.1}$$

see (3.4) and figure 4, where the interpolation kernel χ depends on *a priori* assumptions on the largest semiclassical wave front set $\mathrm{WF}_h(\mathcal{R}f)$ (which in turn depends on similar assumptions on $\mathrm{WF}_h(f)$), and on s, see section 3.

Assume that $\mathrm{WF}_h(\mathcal{R}f)$ restricts the dual variable $\hat\varphi$ to $|\hat\varphi| \leqslant B' < B$ with some semiclassical band limit B, where B is fixed to allow for some degree of oversampling below. *A priori*, B' can be very close to B, and B/B' can be considered as the degrees of oversampling. For lack of aliasing plus the so chosen degree of oversampling, we require $s \leqslant \pi/B$ (the Nyquist conditions), the interpolation functions to be smooth, to satisfy $\operatorname{supp}\hat\chi \subset [-\pi,\pi]$, and $\hat\chi(\hat\varphi) = 1$ for $|\hat\varphi| \leqslant \pi B'/B$. Then (6.1) provides an approximation of $\mathcal{R}f$ up to an $O(h^\infty)$ error, see section 3.

The critical case of no-oversampling ($B' = B$), which we do not allow, requires interpolation functions $\chi(s) = \operatorname{sinc}(\pi x)$, where $\operatorname{sinc}(x) = \sin x/x$. This function decays slowly and in practical implementations it is often replaced by a kernel with a compact support extending over only a few neighboring points. On the other hand, with some oversampling, we can (and we did) chose χ to be of Schwartz class. A practical choice of a interpolation kernel satisfying the requirements approximately is the Lanczos-3 interpolation kernel

$$\mathrm{Lan3}(x) := h_0(3 - |x|)\operatorname{sinc}(\pi x)\operatorname{sinc}(\pi x/3), \tag{6.2}$$

where h_0 is the Heaviside function. While the Fourier transform of $\operatorname{sinc}(\pi x)$ is the characteristic function of $[-\pi,\pi]$, the Fourier transform of Lan3 is essentially (but not exactly, of course) supported in twice that interval but it is very close to 1 in a half of it: in $[-\pi/2,\pi/2]$, see [38]. Therefore, Lan3 would lead to some aliasing but it will preserve most of the non-aliased frequencies. On the other hand, if we use $\mathrm{Lan3}(x/2)$ instead, its Fourier transform satisfies the requirements approximately with a degree of oversampling approximately 2, while attenuating frequencies with magnitudes in $[-\pi/2,\pi]$. The resulting interpolation (6.1) then would be $\mathcal{R}f$ with a low pass filter applied, up to an $O(h^\infty)$ error.

Note that $\mathcal{H}$ could be applied before or after the interpolation (6.1) with the same result. The inversion in this case would be

$$f_{\psi,\chi} := \mathcal{R}'\mathcal{H}g_{\rm int}. \tag{6.3}$$

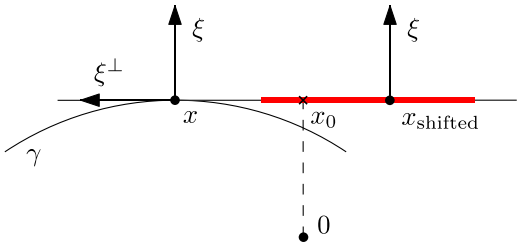

Figure 5. Aliasing with the interpolation method: (x,ξ) shifts to (x_{shifted},ξ) along the line tangent to γ at x. The point x_{shifted} can be at distance at most $d/3$ to the left and d to the right of x_0, where $d=|x-x_0|$.

As mentioned above, by [37], if $\operatorname{supp} f\subset\mathcal{B}(0,R)$, the sharp condition for avoiding aliasing, is

$$s<\pi/(RB), \tag{6.4}$$

where B is the band limit for f_h. In that case, one can reconstruct $\mathcal{R}f$ up to $O(h^\infty)$ by (6.1), and then f. If $s<\pi/(2RB)$ (oversampling by a factor of two), one can use the Lanczos-3 interpolation which is local and much more practical, to achieve great accuracy. When (6.4) does not hold, and one still uses the same reconstruction, aliasing occurs. The aliasing artifacts appear as a sum of h-FIOs with canonical relations which happen to be the same as (5.4), when

$$x\cdot\xi^\perp+2k\pi/s\in[-\pi/s,\pi/s], \tag{6.5}$$

(and we relabeled them by changing the sign of k compared to [37]). If (6.4) holds, we have $|x\cdot\xi^\perp|<RB<\pi/s$, thus (5.4) can hold with $k=0$ only, hence no aliasing.

By (5.10), k depends on (x,ξ). Note that for each (x,ξ) with $\xi\neq 0$, there is unique k satisfying (5.10) with the exception of the case when the left-hand side happens to be an endpoint on the interval on the right; but then $\hat\chi$ kills the interpolation for such frequencies because we assume $\operatorname{supp}\hat\chi_\varphi\subset[-\pi,\pi]$. On the other hand, if we use the Lanczos-3 kernel, which does not satisfy this condition, even approximately (but it does in $[-2\pi,2\pi]$, as explained above), we can get two aliased artifacts.

In figure 5, we illustrate this analysis for a singularity (x,ξ), say conormal to a smooth curve γ (which is not important). We have $x\cdot\xi^\perp>0$, so if aliasing happens, we must have $k<0$ in (5.10). Then that (x,ξ) would shift along the ray issued from x tangent to the curve γ, in the direction $-\xi^\perp$, i.e. towards the point on that tangent line closest to the origin. The jump at γ may create a singularity at $(x,-\xi)$ as well but then $k>0$ and the artifact would still appear on the same ray.

A closer inspection of conditions (5.4) and (5.10) reveals that the aliased images of (x,ξ) may appear at points x over some interval over that tangent line only. Indeed, condition (5.10) is equivalent to

$$-x\cdot\xi^\perp\in[(2k-1)\pi/s,(2k+1)\pi/s]. \tag{6.6}$$

Then x is displaced along the line through x in the direction of $\xi^\perp$ by $2\pi k/(s|\xi|)$, and for the shifted x we have

$$-\left(x+\frac{2\pi k}{s}\frac{\xi^\perp}{|\xi|^2}\right)\cdot\frac{\xi^\perp}{|\xi|}\in\frac{1}{|\xi|}[-\pi/s,\pi/s].$$

Write $x\cdot\xi^\perp = x\cdot(\xi^\perp/|\xi|)|\xi|$ in (6.6), and determine the range of $|\xi|$ with $\xi/|\xi|$ fixed, assuming first $-x\cdot\xi^\perp>0$, hence $k>0$. We see then that x can shift along the line through x in the direction $\xi^\perp/|\xi|$ within the range of the signed distances

$$-\frac{x\cdot\xi^\perp}{|\xi|}\left[\frac{2k}{2k+1},\frac{2k}{2k-1}\right],\quad k=1,2,\dots,\quad x\cdot\xi^\perp>0, \tag{6.7}$$

where we used the convention $k(a,b)=(ka,kb)$. When $-x\cdot\xi^\perp<0$ (then $k<0$), we get the same conclusion just by replacing ξ by $-\xi$, and k by $-k$. Thus (6.7) holds for $k<0$, as we indicated above. In figure 5, we have $k=-1$.

The largest of the intervals in the square brackets in (6.7) is $[2/3,2]$. The upper bound of the distance $2|x\cdot\xi^\perp|/|\xi|$ is achieved right when aliasing occurs, i.e. when $k=1$ in (5.10) and the l.h.s. approaches $-\pi/s$. If we keep the direction of ξ the same but increase its magnitude, the aliased singularity moves closer to x until it gets at distance $(2/3)|x\cdot\xi^\perp|/|\xi|$. Then it jumps to $4/3$ of that factor, moves to $4/5$, etc. In the end, the minimal interval is $[2/3,2]$. Therefore, we have the following.

Theorem 6.1. *Under the conditions of theorem 5.2, statements (a) and (b) there are preserved for $f_{\psi,\chi}$. Instead of an equality in (c), we have*

$$\mathrm{WF}_h(f_{\psi,\chi})\setminus 0\subset\left\{x-\left[\frac{2}{3},2\right]\frac{x\cdot\xi^\perp}{|\xi|}\frac{\xi^\perp}{|\xi|},\ (x,\xi)\in\mathrm{WF}_h(f_\psi)\setminus 0\right\}. \tag{6.8}$$

6.2. Translation non-invariance and refocusing

One of the consequences of the analysis in [37] is that the resolution, defined there, is inversely proportional to $|x|$ (and also direction dependent). This is also consistent with (6.4), where $R\ll 1$ allows $B\gg 1$ for the same step s. This makes the origin a special point, with the resolution near it the highest. In a way, the interpolation method is 'focused' at the origin. It is easy to see that the parallel geometry parameterization is not invariant under translations and rotations in the sense that it does not preserve its form. Rotations $x\mapsto Ux$ are innocent; they just transform ω into $\tilde\omega:=U^*\omega$. In (2.2), this corresponds to shifting φ (and still considering in modulo 2π). Shifting x by $\tilde x=x-x_0$ however, changes the type of the equation $x\cdot\omega(\varphi)=p$ to

$$\tilde x\cdot\omega(\varphi)=p-x_0\cdot\omega(\varphi). \tag{6.9}$$

Setting

$$\tilde p=p-x_0\cdot\omega(\varphi), \tag{6.10}$$

we get a pseudo-parallel parametrization but $\tilde p$ depends on φ now. This is reasonable to expect: each time we choose an angle φ, we are free to put the origin on the line $\omega(\varphi)^\perp$ parameterizing the lines with that direction, anywhere we want to. In (2.1), the choice happens to correspond to the line through the origin in the x-plane. This makes the origin a special point without any need to be such. We are free to change that parameterization to (6.9), for example, to even do something different, choosing $\tilde p$ to be a more general function of φ.

That freedom does not do much when we have $\mathcal{R}f(\omega,p)$ for all ω and p (or for them in some open set). In the discrete setting however, things change. We will call the re-parameterization (6.10) *refocusing*. If we know $\mathcal{R}f(\omega,p)$ for ω in a discrete set (and all p), we can perform (6.10) for each such ω, and x_0 fixed. This would map the curve $x_0\cdot\omega=p$, see figure 4 into the straight line $\tilde p=0$. Then the inversion would look like x_0 were the origin, which would move the aliasing artifacts elsewhere! Recall that we assume a high enough sampling rate s_p in the p variable, which makes implementing (6.10) easy.

6.3. Relation between the two methods

Finally, we show that the interpolation reconstruction operator is just the 'direct' one convolved in the ω variable with the interpolating function.

Theorem 6.2. *For every $f\in C_0^\infty(\mathbb{R}^2)$ and $\psi\in\mathcal{S}(\mathbb{R})$, a*

$$f_{\psi,\chi}(r\omega(\theta))=\chi_{sh}*_\theta f_{\psi,\delta}(r\omega(\theta)),$$

where $*_\theta$ is the circular convolution in the θ variable, and $\chi_h(\theta)=h^{-1}\chi(\theta/h)$.

Proof. By (6.1) and (6.3),

$$f_{\psi,\chi}(x)=\int\sum_j\psi(jsh)(\mathcal{H}\mathcal{R}f)(\omega(jsh),x\cdot\omega(\varphi))\chi\Big(\frac{\varphi-jsh}{sh}\Big)\mathrm{d}\varphi.$$

Write $x=r\omega(\theta)$, and make the change of variables $\tilde\varphi=\varphi-jsh$. Since $x\cdot\omega(\tilde\varphi+jsh)=r\omega(\theta)\cdot\omega(\tilde\varphi+jsh)=r\omega(\theta-\tilde\varphi)\cdot\omega(jsh)$, we get

$$f_{\psi,\chi}(r\omega(\theta))=sh\int\sum_j\psi(jsh)(\mathcal{H}\mathcal{R}f)(\omega(jsh),r\omega(\theta-\tilde\varphi)\cdot\omega(jsh))\chi_{sh}(\tilde\varphi)\,\mathrm{d}\tilde\varphi.$$

This is exactly the circular convolution of (5.1) with χ_{sh} as claimed. □

The convolution in theorem 6.2 is a Fourier multiplier in polar coordinates, in the angular variable, with $\mathcal{F}_h\chi_s$. Passing back to the Cartesian coordinates, we get an h-ΨDO with principal symbol $\chi_s(-x^2\xi_1+x^1\xi_2)$ at least away from $x=0$. This shows that the two reconstructions are related by an h-ΨDO, and since we showed in theorem 5.1 that $f_\psi\mapsto f_{\psi,\delta}$ is an h-FIO, it now follows that $f_\psi\mapsto f_{\psi,\chi}$ is an h-FIO with the same canonical relation, something we proved directly in theorem 6.1.

6.4. Comparison of the two methods

We managed to get from the discrete measurements g_j (2.5) to 'continuous' ones with the aid of the Poisson summation formula (4.12). We will offer here an alternative point of view.

We can think of the numerical integration formula (4.4) in the following way. First, we interpolate the discrete data somehow with an interpolation kernel χ having total integral one. We do that for each x, along the curve $\varphi\mapsto(\omega(\varphi),x\cdot\omega(\varphi))$, see figure 1. Then integrating the interpolated function removes χ and reduces to the finite sum (4.4).

The interpolation method, on the other hand, interpolates horizontally in figure 1, i.e. along the lines $\varphi\mapsto(\omega(\varphi),p=\text{const.})$. Only one of those lines coincides with some of the lines above: the line $p=0$ (in the (φ,p) plane, more precisely, on the cylinder $S^1\times\mathbb{R}$), which corresponds to all lines in the x plane through $x=0$. The two methods are equivalent, roughly speaking, in an infinitesimal neighborhood of $x=0$, as theorem 6.2 indicates as well. Away from $x=0$, $f_{\psi,\chi}$ is just an angularly blurred version of $f_{\psi,\delta}$. The advantage of the direct method is that the interpolation before integration (which is not needed, as explained above) is x-dependent. In that sense, that method focuses at every point x to evaluate $f_{\psi,\delta}$ there.

7. Recovery of an edge and aliasing from an edge, classical view

Assume that f is piecewise smooth with a jump over a smooth curve (an 'edge') near some point x_0, and has no other singularities. We want to understand how well the edge is resolved,

and what kind of aliasing artifacts are created. We want to emphasize that if f has other singularities, they may create aliasing artifacts near x_0 as well, interfering with the ones we analyze here. This problem has been studied in the literature for special shapes, at least. For example, the cases of f being a characteristic function of an elliptical domain or of a square are explicitly computed in [5, pp 473–6], see also the references there, and [32, 35].

Assume that we use the direct method, formula (4.2), which is also (4.4) when we restrict our attention to lines close to being tangent to the edge, and $\psi = 1$ there. It is enough to analyze each summand in (4.2) independently. We are going to analyze three cases which do not exhaust all possible ones. In this section, $h = 1$, i.e. we do not take the angular step to be a small parameter, respectively m is fixed. We study the direct method here only.

7.1. A flat edge

Assume that the edge is flat neat x_0. Then the recovered f_δ depends on whether that edge is normal to some of the ω_j's (i.e. parallel to some of the lines in our family) or not; and in the latter case, it will depend to the distance of its normal to $\{\omega_j\}$.

Assume first that the edge is normal to ω_{j_0} for some j_0. Then $\mathcal{R}f(\omega_{j_0}, p)$ would have a jump-type of singularity at some $p = p_0$, and $\mathcal{R}f(-\omega_{j_0}, p)$ would have a jump-type of singularity at $p = -p_0$. Without loss of generality, we can assume that it is the former term appearing in (4.2). Then $\mathcal{H}\mathcal{R}f(\omega_{j_0}, p)$ would be a distribution but not a (locally L^1) function! Indeed, writing $\mathcal{R}f(\omega_{j_0}, p) = kh_0(p - p_0)$, $k \neq 0$, modulo higher regularity terms (which regularity depends on the behavior of f near that edge), where h_0 is the Heaviside function, one needs to understand $\mathcal{H}\mathcal{R}f(\omega_{j_0}, p) \sim k\mathcal{H}h_0(p - p_0)$. Therefore, the leading singularity of f_δ would be expected to be (ignoring the localization for a moment),

$$\frac{2\pi}{m} k\mathcal{H}h_0(p - p_0) = \frac{k}{2m} H\mathrm{d}_p h_0(p - p_0) = \frac{k}{2m} H\delta(p - p_0)$$
$$= \frac{k}{2\pi m}\,\mathrm{pv}\,\frac{1}{p - p_0}, \quad \text{where } p = x \cdot \omega.$$

In (7.1), we provide a more precise statement, and a second term. Note that this is the behavior along the line $x \cdot \omega_{j_0} = p_0$ independently of whether the point on that line is on the actual edge or not. The result is a distribution. All other terms in (4.2) would contribute smooth terms, so this describes all leading order singularities of f_δ under our assumptions.

If the edge is not normal to any ω_j, then f_δ would be smooth. When the edge is 'almost normal' to some ω_j however, there will be a steep change across that line.

In figure 6, we demonstrate this behavior. The computations are done in a 1000×1000 grid. The angular step is 10°, with the vertical direction being among the set of the directions (corresponding to $\varphi_1 = 0$ being the first one). The reason the bright phantom looks so pale in (b) is that the range has been adjusted from $[0, 1]$ in (a) to $[-2.1, 2.7]$. Two cross-sections, marked with small horizontal bars in (b), are plotted. The one through the maximum of the jump actually recovers the edge well, plus a $\mathrm{pv}(1/x)$ type of singularity as predicted. The edge is well recovered because the contributions from the lines with directions close to vertical are smooth but sharply changing near the edge. This is better understood in asymptotic sense, when the angular step size gets smaller and smaller, as we do later. The second cross-section is near the bottom of the square, where the jump is zero, and what is left is a $\mathrm{pv}(1/x)$ singularity.

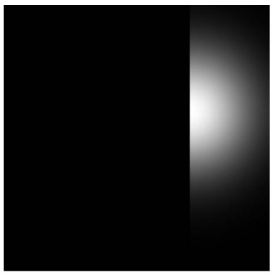

(a) A flat edge.

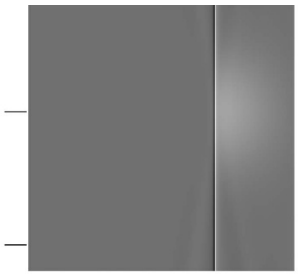

(b) Recovered, angular step 10°.

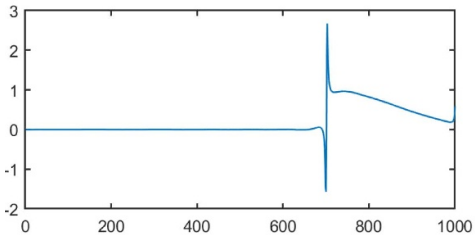

(c) A horizontal cross-section plot across the maximal jump; the top bar in (b).

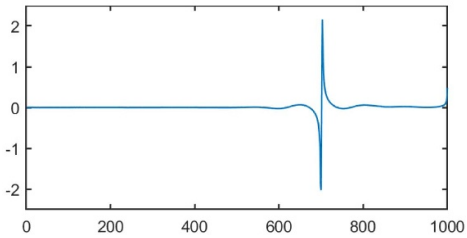

(d) A horizontal cross-section plot near the bottom; the bottom bar in (b).

Figure 6. A flat edge with $s = 10^\circ$ with $\mathrm{pv}(1/x)$ singularities visible in the reconstruction. Near the actual edge, the jump is recovered well but this is due to smooth but sharply changing contributions from close non-tangent lines.

7.2. A strictly convex/concave edge

Assume that the edge is strictly convex or concave, depending on the direction at which we are looking, i.e. it is a smooth curve with nonzero curvature near x_0. Then $\mathcal{R}f$ would have singularities at lines tangent to the edge, where f jumps. Fixing one such direction, $\mathcal{R}f(\omega,p) \sim kh_0(p-p_0)_+^{1/2}$, where $t_+ = \max(t,0)$, $t_- = (-t)_+$, $k = 2\sqrt{2}f(x_0)/\sqrt{|\kappa|}$, and κ is the curvature. Again, without loss of generality we assumed that the curve lies in $p \geqslant p_0$, not $p \leqslant p_0$. As above, we need to understand $\mathcal{H}$ applied to it. This is done in (7.2) in lemma 7.1. We get that f_δ would have conormal singularities along the line determined by (ω_{j_0}, p_0) of the kind

$$-\frac{k}{2\pi m}(p-p_0)_-^{-1/2}$$

as the most singular part of f_δ, near the line $x\cdot\omega_j = p_0$. This is an integrable singularity. A numerical reconstruction is shown in figure 7. The $-x_-^{-1/2}$ singularities are well visible.

7.3. Artifacts from a corner

Let f has a jump across a corner, like $f = h_0(x^1)h_0(x^2)$ near $x = 0$. Then $\mathrm{WF}(f)$ over the corner consists of all directions, which will create singularities conormal to all lines in our set through this corner. To be more precise, assume that we have two smooth curves through x_0, intersecting transversally, so that f is equal to the restriction of a smooth function f_0 with $f_0(x_0) \neq 0$, to one of the four sectors, and zero in the other three. Assume that ω_{j_0} is not normal to either of those curves at x_0. Then $\mathcal{R}(\omega_{j_0}, p) \sim k(p-p_0)_+$ locally, $k \neq 0$, modulo smoother terms. By (7.3) in

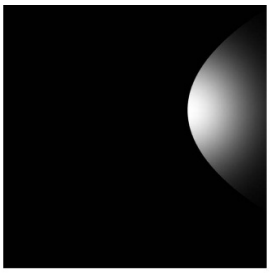

(a) A convex edge

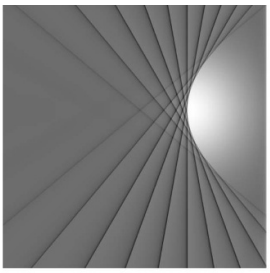

(b) Recovered, angular step 10°.

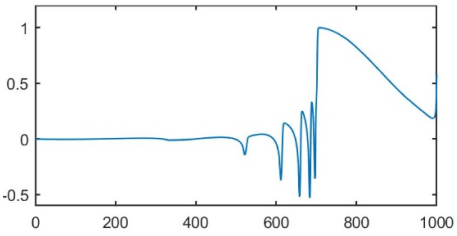

(c) A horizontal cross-section plot of (b) across the maximum of the jump.

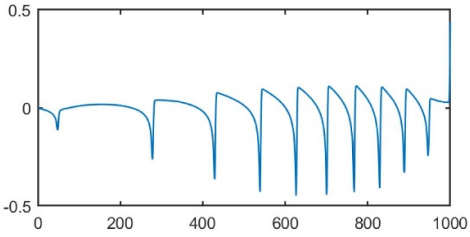

(d) A horizontal cross-section plot of (b) near the bottom.

Figure 7. A convex edge with $s = 10^\circ$ with $-x_-^{-1/2}$ singularities visible in the reconstruction. Near the actual edge, the jump is recovered well but this is due to smooth but sharply changing contributions from close non-tangent lines.

lemma 7.1, f_δ would have conormal singularities along the line determined by (ω_{j_0}, p_0) of the kind

$$\frac{k}{2\pi m}\log|p-p_0|.$$

It is the weakest of the three.

A numerical illustration is presented in figure 8. In (d), we see log type of peaks along a horizontal line staying at 30% from the bottom. Most of them point down, corresponding to $+\log|\cdot|$. They correspond to lines through the corner not entering the sector where $f>0$. The most left one corresponds to a line through the corner entering that sector, and the singularity is of the type $-\log|\cdot|$. This explains why that peak points upwards.

We used the following lemma above.

Lemma 7.1. *Let $\phi\in C_0^\infty(\mathbb{R})$. Then*

$$\mathcal{H}\phi h_0(x) = \frac{1}{4\pi^2}\left(\phi(0)\,\mathrm{pv}\,\frac{1}{x}+\phi'(0)\log|x|\right) \mod C^0(\mathbb{R}), \tag{7.1}$$

$$\mathcal{H}\phi x_+ = \frac{1}{4\pi^2}\phi(0)\log|x| \mod C^0(\mathbb{R}), \tag{7.2}$$

$$\mathcal{H}\phi x_+^{\frac{1}{2}} = -\frac{1}{4\pi^2}\phi(0)x_-^{-\frac{1}{2}} \mod C^0(\mathbb{R}). \tag{7.3}$$

Proof. The lemma is a computation of a singularity conormal at $x=0$ under the action of the ΨDO $\mathcal{H}=(4\pi)^{-1}|D|$. The result is given by [14, theorem 18.2.12]. In our case, a (compactly supported) conormal distribution in $\mathbb{R}$ at $x=0$ of order m is given by

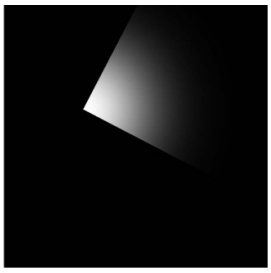

(a) A corner

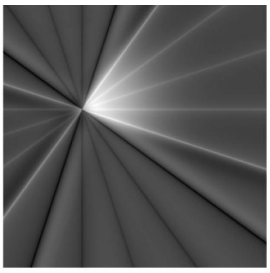

(b) Recovered, angular step 18°.

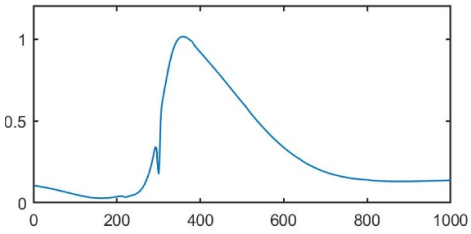

(c) A horizontal cross-section plot near the tip.

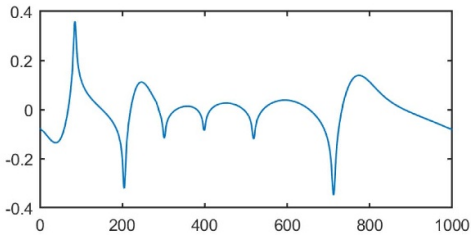

(d) A horizontal cross-section plot near the bottom.

Figure 8. A corner with $s = 18^\circ$ with $\pm\log|x|$ singularities visible in the reconstruction. Near the actual edge, there is a similar singularity as well plus a blurred version of the jump, which is one.

$$u(x) = \frac{1}{2\pi}\int e^{\mathrm{i}x\xi}a(\xi)\,\mathrm{d}\xi,$$

i.e. just the inverse Fourier transform of a, where a is a symbols of order $m+1/4$. Applying various smooth cutoffs to u which are equal to one near $x=0$ may change the symbol only up to a term of order $-\infty$. If ϕ does not satisfy that, the symbol would be modified depending on the Taylor expansion of ϕ at zero. The distributions in the lemma are not compactly supported before multiplying by ϕ but they are homogeneous, thus they have homogeneous Fourier transforms singular at $\xi=0$ only. One can see that a multiplication by $\phi(x)$ would produce a compactly supported conormal distribution with a symbol equal to those Fourier transforms, up to $O(|\xi|^{-\infty})$.

Applying a ΨDO $p(x,D)$ of order m' to a conormal distribution of order m in our case produces a conormal distribution at $x=0$, again of order $m+m'$, with complete symbol

$$\sum\langle -\mathrm{i}D_x, D_\xi\rangle^j p(x,\xi)a(\xi)/j!|_{x=0}, \tag{7.4}$$

see, e.g. [14]. In our case, $p(x,D) = (4\pi)^{-1}|D|\phi(x)$, i.e. it has an amplitude $a(x,y,\xi) = (4\pi)^{-1}|\xi|\phi(y)$. For its symbol $p(x,\xi)$ we have

$$4\pi p(x,\xi) = \phi(x)|\xi| - \mathrm{i}\phi'(x)\operatorname{sgn}\xi\,.$$

The symbol of the Heaviside function h_0 is $-\mathrm{i}/\xi$ (away from $\xi=0$), therefore, in (7.4), we have

$$4\pi p(x,\xi)a(\xi) = -\mathrm{i}\phi(x)\operatorname{sgn}\xi - \phi'(x)\operatorname{sgn}\xi/\xi\,. \tag{7.5}$$

By (7.4), the symbol of the conormal distribution $4\pi\phi h_0$ then is

$$4\pi p(x,\xi)a(\xi) = -\mathrm{i}\phi(0)\operatorname{sgn}\xi - \phi'(0)\operatorname{sgn}\xi/\xi + \mathrm{i}\phi''(0)\operatorname{sgn}\xi/\xi^2 \mod S^{-3}. \tag{7.6}$$

Now, $-\mathrm{i}\operatorname{sgn}\xi$ is the symbol (the Fourier transform) of $\pi^{-1}\operatorname{pv}(1/x)$. Next, $-\operatorname{sgn}\xi/\xi$ is the symbol of the distribution with derivative having symbol $-\mathrm{i}\operatorname{sgn}\xi$, which is $\pi^{-1}\operatorname{pv}(1/x)$. Taking antiderivative of the latter, we get $\pi^{-1}\log|x|$. Finally, $\mathrm{i}\operatorname{sgn}\xi/\xi^2$ is obtained from $-\mathrm{i}\operatorname{sgn}\xi$ by multiplying by $-1/\xi^2$, which corresponds to taking the second antiderivative; hence we get $\pi^{-1}x(\log|x|-1)$, which is a continuous function. The latter also follows from the fact that a symbol $\sim 1/\xi^2$ at $\xi\to\infty$ is L^1 there, therefore, its inverse Fourier transform is continuous. By the same argument, the remainder in (7.6) produces a C^1 function, and one can get a complete singular expansion, in fact. This proves (7.1) in the lemma.

Equation (7.2) follows in a similar way. The symbol of the conormal distribution $a(\xi) = x_+$ is $-1/\xi^2$, therefore in (7.5) we have

$$4\pi p(x,\xi)a(\xi) = -\phi(x)/|\xi| + \mathrm{i}\phi'(x)\operatorname{sgn}\xi/\xi^2$$

instead. The second term produces a continuous function while the first one, by the calculations, above, would produce a leading term $\pi^{-1}\phi(0)\log|x|$ plus another continuous function.

For the last identity (7.3) in the lemma, we need the symbol of $x_+^{1/2}$. Since $\mathcal{H} = (4\pi)^{-1}|D| = (4\pi)^{-1}H\mathrm{d}/\mathrm{d}x$, dropping the factor $(4\pi)^{-1}$ for a while, we can apply $\mathrm{d}/\mathrm{d}x$ first to study $x_+^{-1/2}$. We have

$$(x_+^{\lambda-1})\hat{} = \Gamma(\lambda)\left(e^{-\mathrm{i}\pi\lambda/2}\xi_+^{-\lambda} + e^{\mathrm{i}\pi\lambda/2}\xi_-^{-\lambda}\right), \quad \lambda\notin\mathbb{Z},$$

see, e.g. [7, chapter 8.6]. When $\Re\lambda > 0$, $x_+^{\lambda-1}$ is locally integrable and in general, it is defined by analytic extension in λ. Therefore, with $\lambda = 1/2$,

$$(x_+^{-1/2})\hat{} = \sqrt{\pi}\left(e^{-\mathrm{i}\pi/4}\xi_+^{-1/2} + e^{\mathrm{i}\pi/4}\xi_-^{-1/2}\right).$$

Then H is a multiplication with $-\mathrm{i}\operatorname{sgn}(\xi)$ on the Fourier side, which happens to make sense on $x_+^{-1/2}$, hence

$$\begin{aligned}(Hx_+^{-1/2})\hat{} &= -\mathrm{i}\sqrt{\pi}\left(e^{-\mathrm{i}\pi/4}\xi_+^{-1/2} - e^{\mathrm{i}\pi/4}\xi_-^{-1/2}\right)\\ &= -\sqrt{\pi}\left(e^{\mathrm{i}\pi/4}\xi_+^{-1/2} - e^{\mathrm{i}3\pi/4}\xi_-^{-1/2}\right)\\ &= -\sqrt{\pi}\left(e^{\mathrm{i}\pi/4}\xi_+^{-1/2} + e^{-\mathrm{i}\pi/4}\xi_-^{-1/2}\right) = -(x_-^{-1/2})\hat{}.\end{aligned}$$

Therefore, $Hx_+^{-1/2} = -x_-^{-1/2}$.

We can use this calculation in (7.4), where $a(\xi) = (x_+^{1/2})\hat{}$ to prove (7.3). The next (continuous) term as a square root singularity, which we will not investigate. □

8. Recovery of edges, an asymptotic view

8.1. The direct method

Recovery of edges will be analyzed here based on theorems 5.1 and 5.2. In the numerical examples in the previous section, we can see that besides the aliasing artifacts creating specific singularities along the edge, the actual jump looks well recovered. The horizontal profiles there are a Gaussian cut by half by the Heaviside function, which creates a jump of size one. In

figure 6(c), one can see a jump one with $C\mathrm{pv}(1/x)$ added. In figure 7(c), if we average the $x_-^{-1/2}$ oscillations on the left, the jump is still close to one. Finally, in figure 8(c), the (weaker) $\log|x|$ singularity is added to a smoothened out cut-off Gaussian with a jump close to one, as well. As explained in that section, removing the predicted singularities, what remains is a continuous function, so the jumps are smoothened out. The reason they appear close to actual jumps in those numerical examples is that the angular step size is not 'too small' but it is still 'small.' If we increase it, the jumps do not look well recovered anymore.

The observed effect is better understood, in author's view, asymptotically, as the angular step size tends to zero. As explained earlier, we assume now that $f = f_h$ is a semiclassically band limited function with bound B.

We start with a general observation which we will not formalize as a theorem. Consider a jump type of singularity. Locally, after a change of variables, it is a multiple of the Heaviside function $h_0(x_2)$ in the x_2 variable, modulo lower order terms. To account for the localization, we represent it as $f = \phi(x)h_0(x_2)$ with some $\phi \in C_0^\infty$. It is convenient to assume that $\phi(x) = \phi_1(x_1)\phi_2(x_2)$. Then

$$\hat f(\xi) = \hat\phi_1(\xi_1)\hat\phi_2 * \Big(\pi\,\delta(\xi_2) - \mathrm{i.pv}\frac{1}{\xi_2}\Big) = \hat\phi_1(\xi_1)\Big(\pi\,\hat\phi_2(\xi_2) - \mathrm{i}\hat\phi_2 * \mathrm{pv}\frac{1}{\xi_2}\Big).$$

Assuming f smoothened by a convolution with some ψ_h as above, we get

$$\mathcal{F}_h(\psi_h * f)(\xi) = \hat\psi(\xi)\hat f(\xi/h) = -\mathrm{i}\hat\psi(\xi)\hat\phi_1(\xi_1/h)\Big[\hat\phi_2(\cdot) * \mathrm{pv}\frac{1}{\cdot}\Big](\xi_2/h) + O(h^\infty). \tag{8.1}$$

The only rays along which this is not $O(h^\infty)$ in a conic neighborhood are the ones parallel to the ξ_2 direction. Along them, $\xi_1 = 0$ and the expression in the brackets has the asymptotic $\sim h/\xi_2$ for $|\xi_2| > 1/C$, $\forall C$. With this in mind, (8.1) is like $-\mathrm{i}h\hat\psi(0,\xi_2)\hat\phi_1(0)\frac{1}{\xi_2}$ along the axis $\xi_1 = 0$, which matters the most. The factor $\hat\psi(0,\xi_2)$ plays a role of a low pass filter modeling the effect of averaging the measurements. If its cutoff frequency, call it B, satisfies (6.4), then there is no aliasing. When it does not, and this is the case we want to understand, there is aliasing as explained earlier. We get artifacts along the line tangent to the curve where the jump occurs, passing to a point where it happens. It is important to note that the number of non-negligible terms in (5.5), restricted to $\mathcal{B}(0,R)$ is independent of h and depends on B only. The factor h above shows that the aliasing artifacts decrease as h when $h \to 0$.

Numerical example. We take a function jumping from 0 to 1 in a slightly smoothened way, across the parabola $x = 1.5y^2$ in a square of size 2 in the plane. Instead of taking $f = h_0(x - 1.5y^2)$, we replace the Heaviside function by $h_\lambda(t) = \frac{1}{2}(1 + \mathrm{erf}(\lambda t))$, where erf is the 'error function' defined as the normalized antiderivative of the Gaussian e^{-t^2} with $\mathrm{erf}(0) = 0$, and $\lim_{t\to\pm\infty}\mathrm{erf}(t) = \pm 1$. Then h_λ is the Heaviside function convolved with a highly concentrated Gaussian, as $\lambda \gg 1$. Its Fourier transform multiplies $1/(\mathrm{i}\xi)$ (for $\xi \neq 0$) by a Gaussian as well. While that multiplier is not compactly supported, for all computational purposes here, it is. This makes the jump function semiclassically band limited with h proportional to $1/\lambda$. Finally, we localize $f = h_\lambda(x - 1.5y^2)$ by multiplying by a function of compact support equal to one near the vertex.

We take $\lambda = 500$. We perform the computations on a 4000×4000 grid with an angular step of 0.8°. The phantom is shown in figure 9(a). The reconstructed one looks virtually the same with the artifacts barely visible, shown in figure 10 on a different scale. We zoom in at the vertex of the hyperbola in figure 9(b) to compare the original phantom and the reconstruction. The squares shown are approximately 70×70 pixel crops of the 4000×4000 original and of the 4002×4002 recovery, respectively (MATLAB's `iradon` adds a pixel on each side if

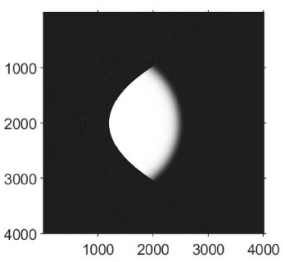

(a) A convex edge

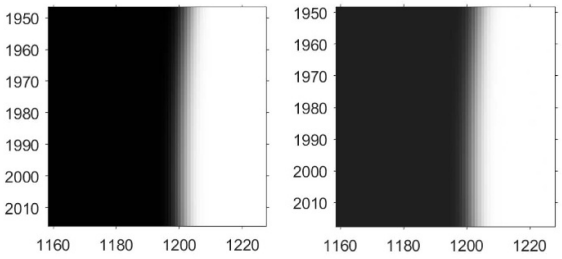

(b) Highly zoomed in: original vs. recovered, $s = 0.8^\circ$.

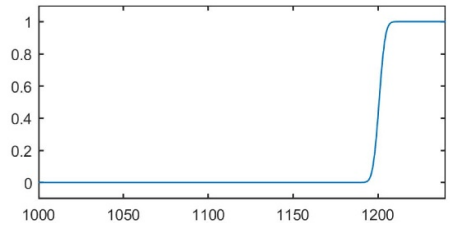

(c) A horizontal cross-section plot of the phantom at the vertex over a small part of the horizontal axis.

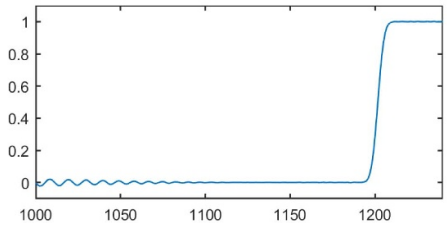

(d) A horizontal cross-section plot of the reconstruction at the vertex..

Figure 9. A convex 'semiclassical edge' with $s = 0.8^\circ$.

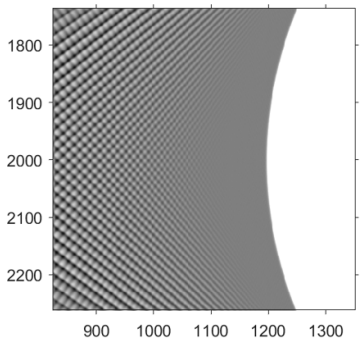

Figure 10. A zoomed in 525×525 crop of the reconstruction in figure 9, with range $[-0.1, 0.1]$, clipping all values $\geqslant 0.1$. A neighborhood of the edge is free of artifacts.

the output size is not specified). In figures 9(c) and (d), we show plots of horizontal cross-sections of the edge through the vertex, well stretched compared to (a), with 6% of the total cross-section plotted. The edge is very will recovered, and the artifacts (the low amplitude oscillations) are separated from the edge at a distance controlled by the effective band limit of f.

Finally, in figure 10, we show an approximately 525×525 crop, zoomed in, of the vertex area rendered to the range of values $[-0.1, 0.1]$ (the original one is $[0, 1]$) to emphasize on the artifacts. We see that in some neighborhood of the edge, there are no artifacts. This is consistent with the cross-section plot in figure 9(c), and with figure 2, right, see also remark 5.2.

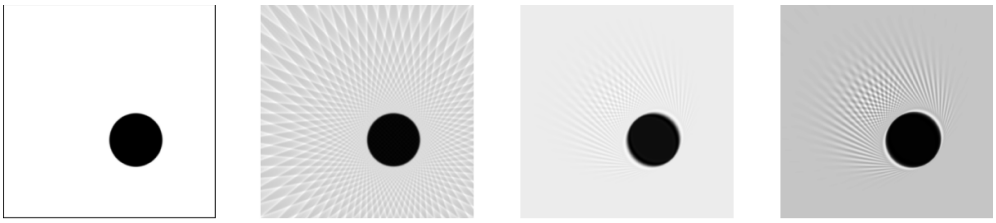

(a) The original f (b) Direct inversion with a 5° step (c) Interpolated inversion with a 5° step (d) As (c) with contrast enhanced

Figure 11. A function f with a jump type singularity and its recovered version from $\mathcal{R}f$ sampled with a 5° step in (a) and (b); and a 3° step in (c) and (d). The origin is in the center.

Compared to the situation on section 7, we have an artifact free neighborhood (in the case of convex edges), and the semiclassical singularities not extending too far from a point. Also, those are semiclassical singularities, high oscillations instead of being classical one.

8.2. The interpolation method

We comment briefly on the recovery of edges with the interpolation method using theorem 6.1. In figure 11, we present a numerical example with a characteristic function, slightly blurred, of a disk placed off center. The conversion in (b) is the direct one. The artifacts are separated from the edge and extend everywhere. The reconstruction in (c) is the interpolated one, and the aliasing artifacts are localized in accordance with theorem 6.1 and figure 5. In (c), we plot a version with an enhanced contrast.

Note that in (c) and in (d), parts of the edge are more blurred than the original, and some oscillations (Gibb's like effect) are visible. The explanation is that when an artifact is created, that frequency is removed from the edge, since for each of them, only one k is possible in (5.4), (5.10). We used the Lanczos-3 interpolation here, which has an oscillating kernel. This, and theorem 6.2 explain why those edges have oscillations when reconstructed. The effect is stronger for the edges with tangents passing through the origin since they would be most affected by the angular convolution.

Data availability statement

This is a math paper, no data collected. The data that support the findings of this study are available upon reasonable request from the authors.

Appendix. Sampling on the unit circle

The circle is a manifold, with no unique chart possible (but two suffice). The definition of a (classical) band limit is not invariant under coordinate changes but is invariant under rigid motions, so it requires some clarification what it means on the unit circle. Note that in contrast, the semiclassical band limit is based on $\mathrm{WF}_h(f)$, which is defined by localization first, thus it is well defined assuming angular parameterization.

Let f be a function on the unit circle. We can think of it as a function of the polar angle φ, periodic with period 2π. The natural Fourier transform is an expansion in Fourier series. On

the other hand, there are natural coordinate maps on the unit circle preserving the arc-length. We can remove any fixed point x_0 from it, say having a polar angle $\varphi_0 \mod 2\pi$ and map the rest to $(\varphi_0, \varphi_0 + 2\pi)$ by the polar angle. Given a distribution f on S^1, depending on h, we can localize it to that chart by a smooth cut-off χ.

Definition A.1. If χf is semiclassically band limited for every such chart, we call f semiclassically band limited with band limit B being the supremum of the band limit over all such charts.

Lemma A.1. *The supremum B in definition A.1 is finite. Moreover, $B = \max(B_1, B_2)$, where B_1, B_2 are two such band limits for two charts corresponding to two distinct cut-off points, and the corresponding χ_1, χ_2 form a partition of unity.*

Proof. For every distribution on S^1, we can write $f = \chi_1 f + \chi_2 f$. Let $x_0 \in S^1$ with a polar angle $\varphi_0 \mod 2\pi$ be a cut-off point for a local chart. Let $\chi_0 \in C^\infty(S^1)$ be zero near x_0. Then $\chi_0 f = \chi_0\chi_1 f + \chi_0\chi_2 f$. The term $\chi_0\chi_1 f$ can be written as a sum of two functions: one supported between x_0 and x_1 (going in positive direction along the circle), and the other one supported between x_1 and x_0. They both can be re-mapped to the chart associated with x_1 at the expense of possible shifting by $2\pi k$, $k \in \mathbb{N}$. That shift does not change the semiclassical band limit, and a multiplication by a C_0^∞ function cannot make it greater; therefore, the semiclassical band limit of $\chi_0\chi_1 f$ does not exceed B_1. We analyze $\chi_0\chi_2 f$ in the same way to get an upper bound B_2. Therefore, an upper bound is $B = \max(B_1, B_2)$ but since it is attained for either $\chi_1 f$ or $\chi_2 f$, it is actually the least one. □

Definition A.2. The function $f_h \in C^\infty(S^1)$ is called semiclassically band limited with band limit B, if (i) it is tempered, i.e. $\|f_h\|_{L^2(S^1)} \leqslant Ch^{-N}$ for some N, (ii) and for its Fourier coefficients f_n, for each $B' > B$, we have

$$|f_n| \leqslant C_N |n|^{-N}, \quad |n| > B'/h. \tag{A.1}$$

Proposition A.1. *Definitions A.1 and A.2 are equivalent.*

Proof. Let f be a semiclassically band limited with a band limit B, according to definition A.1. Since χf is tempered for any cutoff χ as in definition A.1, we deduce that f is tempered, too. The Fourier coefficients of f are given by

$$f_n = \int_0^{2\pi} e^{-in\varphi} f(\omega(\varphi))\, \mathrm{d}\varphi.$$

We view the integration above as an integration over S^1 since $e^{-in\varphi}$ is 2π-periodic. Then we apply the partition of unity $1 = \chi_1 + \chi_2$ to f as in lemma A.1. The integral of each term resulting from that can be written as an integral over a subinterval of the real line. It is enough to consider the first one only. We have

$$\int_{\varphi_1}^{\varphi_1 + 2\pi} e^{-i\varphi\,(hn)/h} (\chi_1 f)(\omega(\varphi))\, \mathrm{d}\varphi.$$

This is the semiclassical Fourier transform of $\chi_1 f$ evaluated at $\hat\varphi = hn$. It is $O(h^N \langle\hat\varphi\rangle^{-N})$ for every N, and for $|\hat\varphi| > B' > B$, which implies $O(h^N(1 + h|n|)^{-N})$, hence $O(1 + |n|)^{-N}$ for $|n| > B'/h$.

Assume definition A.2 now. Then f is tempered and we have (A.1). Write

$$f(\varphi) = \frac{1}{2\pi} \sum e^{in\varphi} f_n.$$

For $\chi \in C_0^\infty$,

$$\mathcal{F}_h \chi f(\hat{\varphi}) = \frac{1}{2\pi} \sum_{n=-\infty}^{\infty} f_n \hat{\chi}(\hat{\varphi}/h - n). \tag{A.2}$$

Choose $B' > B'' > B$ and restrict $\hat{\varphi}$ to $|\hat{\varphi}| > B'$. Notice first that

$$|\hat{\chi}(\hat{\varphi}/h - n)| \leqslant C_N |\hat{\varphi}/h - n|^{-N} = C_N h^N |\hat{\varphi} - hn|^{-N}. \tag{A.3}$$

Summing over $|n| \leqslant B''/h$ in (A.2), we get

$$\left| \sum_{|n| \leqslant B''/h} f_n \hat{\chi}(\hat{\varphi}/h - n) \right| \leqslant C_N' h^N |\hat{\varphi}|^{-N} \quad \text{for } |\hat{\varphi}| > B', \tag{A.4}$$

where we used (A.3), and the fact that the number of terms above is $O(h^{-1})$. For the remainder of the sum, we have

$$\left| \sum_{|n| > B''/h} f_n \hat{\chi}(\hat{\varphi}/h - n) \right| \leqslant C_N \sum_{|n| > B''/h} |n|^{-N-2} |\hat{\chi}(\hat{\varphi}/h - n)|. \tag{A.5}$$

We want to show that it is $O((h/|\hat{\varphi}|)^N)$, $\forall N$. We will multiply by $(\hat{\varphi}/h)^N = \big((\hat{\varphi}/h - n) + n\big)^N$ and show that it is uniformly bounded. Using the binomial formula, we just need to show that multiplying (A.5) by $n^{N-k}(\hat{\varphi}/h - n)^k$, $0 \leqslant k \leqslant N$, leaves it uniformly bounded. Since $\hat{\chi}$ is Schwartz class, it is enough to estimate

$$\sum_{|n| > B''/h} |n|^{-N-2} |n|^{N-k} = \sum_{|n| > B''/h} |n|^{-2} |n|^{-k} \leqslant C.$$

Therefore, (A.5) is $O((h/|\hat{\varphi}|)^N)$, indeed. This, combined with (A.4) shows the same for $\mathcal{F}_j \chi f$ for $|\hat{\varphi}| > B'$, for every fixed $\chi \in C_0^\infty$.

□

Finally, we will mention that on the circle, the sinc interpolation of classically band-limited functions on it (trigonometric polynomials) has its analog as well, see [5].

ORCID iD

Plamen Stefanov https://orcid.org/0000-0002-8544-3411

References

[1] Antoniano J L and Uhlmann G A 1985 A functional calculus for a class of pseudodifferential operators with singular symbols *Pseudodifferential Operators and Applications (Notre Dame, Indiana, 1984)* (*Proc. Symp. in Pure Mathematics* vol 43) (American Mathematical Society) pp 5–16

[2] Borg L, Frikel J, Jørgensen J S and Quinto E T 2018 Analyzing reconstruction artifacts from arbitrary incomplete x-ray CT data *SIAM J. Imaging Sci.* **11** 2786–814

[3] Cormack A M 1978 Sampling the Radon transform with beams of finite width *Phys. Med. Biol.* **23** 1141–8

[4] Dimassi M and Sjöstrand J 1999 *Spectral Asymptotics in the Semi-Classical Limit* (*London Mathematical Society Lecture Note Series* vol 268) (Cambridge University Press)

[5] Epstein C L 2008 *Introduction to the Mathematics of Medical Imaging* 2nd edn (Society for Industrial and Applied Mathematics (SIAM))
[6] Faridani A 2006 Fan-beam tomography and sampling theory *The Radon Transform, Inverse Problems and Tomography* (*Proc. Symp. in Applied Mathematics* vol 63) (American Mathematical Society) pp 43–66
[7] Friedlander F G and Joshi M S 1998 *Introduction to the Theory of Distributions* (Cambridge University Press)
[8] Frikel J and Quinto E T 2013 Characterization and reduction of artifacts in limited angle tomography *Inverse Problems* **29** 125007
[9] Guillemin V and Sternberg S 2013 *Semi-Classical Analysis* (International Press)
[10] Guillemin V and Uhlmann G 1981 Oscillatory integrals with singular symbols *Duke Math. J.* **48** 251–67
[11] Hakkarainen J, Purisha Z, Solonen A and Siltanen S 2019 Undersampled dynamic x-ray tomography with dimension reduction Kalman filter *IEEE Trans. Comput. Imaging* **5** 492–501
[12] Helgason S 1999 *The Radon Transform* (*Progress in Mathematics* vol 5) 2nd edn (Birkhäuser Boston Inc.)
[13] Hörmander L 1983 *The Analysis of Linear Partial Differential Operators. I. Distribution Theory and Fourier Analysis* vol 256 (Springer)
[14] Hörmander L 1985 *The Analysis of Linear Partial Differential Operators. III. Pseudodifferential Operators* vol 274 (Springer)
[15] Huda W and Abrahams R B 2015 X-ray-based medical imaging and resolution *Am. J. Roentgenol.* **204** W393–7
[16] Katsevich A 2017 A local approach to resolution analysis of image reconstruction in tomography *SIAM J. Appl. Math.* **77** 1706–32
[17] Katsevich A 2020 Analysis of resolution of tomographic-type reconstruction from discrete data for a class of distributions *Inverse Problems* **36** 124008
[18] Katsevich A 2020 Resolution analysis of inverting the generalized Radon transform from discrete data in $\mathbf{R}^3$ *SIAM J. Math. Anal.* **52** 3990–4021
[19] Katsevich A 2021 Resolution of 2D reconstruction of functions with nonsmooth edges from discrete Radon transform data (arXiv:2112.10286)
[20] Katsevich A 2022 Novel resolution analysis for the radon transform in $\mathbf{R}^2$ for functions with rough edges (arXiv:2206.04545)
[21] Lemoine C 1972 Fourier transforms of homogeneous distribution *Ann. Sc. Norm. Super. Pisa - Cl. Sci.* **26** 117–49
[22] Louis A K 1981 Ghosts in tomography—the null space of the Radon transform *Math. Methods Appl. Sci.* **3** 1–10
[23] Louis A K 1984 Nonuniqueness in inverse Radon problems: the frequency distribution of the ghosts *Math. Z.* **185** 429–40
[24] Louis A K 2019 Uncertainty, ghosts and resolution in Radon problems *The Radon Transform—The First 100 Years and Beyond* (*Radon Series on Computational and Applied Mathematics* vol 22) (Walter de Gruyter) pp 169–88
[25] Martinez A 2002 *An Introduction to Semiclassical and Microlocal Analysis* (*Universitext*) (Springer)
[26] Mathison C 2020 Sampling in thermoacoustic tomography *J. Inverse Ill-Posed Problems* **28** 881–97
[27] Melrose R B and Uhlmann G A 1979 Lagrangian intersection and the Cauchy problem *Commun. Pure Appl. Math.* **32** 483–519
[28] Monard F and Stefanov P 2022 Sampling the x-ray transform on simple surfaces *SIAM J. Math. Anal.* **55** 1707–36
[29] Natterer F 1986 *The Mathematics of Computerized Tomography* (B. G. Teubner)
[30] Natterer F 1993 Sampling in fan beam tomography *SIAM J. Appl. Math.* **53** 358–80
[31] Nguyen L V 2015 How strong are streak artifacts in limited angle computed tomography? *Inverse Problems* **31** 055003
[32] Ramm A G and Zaslavsky A I 1993 Singularities of the Radon transform *Bull. Am. Math. Soc.* **28** 109–15
[33] Rattey P and Lindgren A 1981 Sampling the 2-D Radon transform *IEEE Trans. Acoust. Speech Signal Process.* **29** 994–1002
[34] Rieder A and Schneck A 2007 Optimality of the fully discrete filtered backprojection algorithm for tomographic inversion *Numer. Math.* **108** 151–75

[35] Shepp L A and Logan B F 1974 The Fourier reconstruction of a head section *IEEE Trans. Nucl. Sci.* **21** 21–43
[36] Stefanov P 2014 The identification problem for the attenuated x-ray transform *Am. J. Math.* **136** 1215–47
[37] Stefanov P 2020 Semiclassical sampling and discretization of certain linear inverse problems *SIAM J. Math. Anal.* **52** 5554–97
[38] Stefanov P and Tindel S 2023 Sampling linear inverse problems with noise *Asymptotic Anal.* **132** 331–82
[39] Zworski M 2012 *Semiclassical Analysis* (*Graduate Studies in Mathematics* vol 138) (American Mathematical Society)